sustainability

MDPI

Article

A Sustainable Hybrid Renewable Energy System for Standalone Sub-Saharan African Areas—A Case Study in Zambia

Satnam Singh Virdy [1], Francis D. Yamba [1], Manish Mishra [2], Isaac N. Simate [3], Mala Ramesh [4,*], Nancy C. Serenje [5] and Mwansa Kaoma [3]

[1] Department of Mechanical Engineering, School of Engineering, University of Zambia, Lusaka 10101, Zambia; svirdy@unza.zm (S.S.V.)
[2] Department of Mechanical Engineering, Indian Institute of Technology, Roorkee 247667, Uttarakhand, India; mmishra@me.iitr.ac.in
[3] Department of Agricultural Engineering, School of Engineering, University of Zambia, Lusaka 10101, Zambia; isaac.simate@unza.zm (I.N.S.); mwansa.kaoma@unza.zm (M.K.)
[4] Department of Electrical and Electronics Engineering, Malnad College of Engineering, Hassan 573202, Karnataka, India
[5] Centre for Energy, Environment and Engineering Zambia, Lusaka 10101, Zambia; nserenje13@gmail.com
* Correspondence: mr@mcehassan.ac.in

Abstract

This study assesses a hybrid photovoltaic/wind/diesel/battery-based renewable energy system in an off-grid area in Zambia. System performance was evaluated through simulation using different photovoltaic panel ratings, battery types, and dispatch strategies. Using the predictive dispatch strategy, the lowest-cost option was a combination of 445 W photovoltaic panels and Li-ion batteries, which had an estimated net present cost of approximately USD 3.857 million over a project lifetime of 25 years, yielding a unit energy cost of USD 0.151/kWh. This system was 73% less expensive than one using a diesel generator, with a 96.4% decrease in emissions and a 95% renewable fraction. Sensitivity analysis revealed that changes in battery price have the greatest impact on operating costs at approximately 12%. The combined methodology using HOMER Pro®Version 3.18 for optimization and MATLAB/Simulink Version R2024b for partial verification of the PV sub-system provides a reproducible framework that can be tailored to other regions facing similar energy challenges. Beyond techno-economic optimization, this study informs sustainable rural electrification planning by evaluating reliability, cost, affordability, lifecycle emissions, and diesel reduction while supporting energy access and climate-resilient off-grid policies in Sub-Saharan Africa.

Keywords: photovoltaic/diesel/battery hybrid system; battery; dispatch strategy; net present cost; sensitivity analysis

Check for updates

Academic Editors: Rohitha Weerasinghe and Sivasakthivel Thangavel

Received: 17 June 2026
Revised: 25 July 2026
Accepted: 28 July 2026
Published: 17 August 2026

Copyright: © 2026 by the authors. Licensee MDPI, Basel, Switzerland. This article is an open access article distributed under the terms and conditions of the Creative Commons Attribution (CC BY) license.

1. Introduction

Uninterrupted access to electricity raises villagers' living standards and improves education, healthcare, and economic activities in local communities. However, increasing demand leads to power crises, placing greater strain on already scarce resources [1]. Samy et al. [2] identify power supply problems facing developing countries, including generation capacity that does not meet demand and unstable grids. Africa, the least electrified continent in the world, is particularly burdened by these challenges [3].

Tazay et al. [4] found that fossil fuels account for approximately 85% of global energy production, increasing emissions and related health problems. Heavy reliance on fossil

fuels can be attributed to the need to supply power to remote locations through grid extension, which is becoming increasingly impractical given limited funds, inadequate energy services, lower grid reliability, and construction challenges [5].

Environmentally friendly technologies for electricity generation are essential for modern energy development and to address the energy supply and sustainability challenges associated with rural electrification [6]. According to Ganjei et al. [7], use of renewable energy sources (RES) is a high priority in several countries and is growing rapidly to meet the electricity needs of off-grid populations. The 2023 SDG Tracking Report states that although the world is advancing towards the United Nations'Sustainability Targets, progress is inadequate [8]. Target 7.1 under Sustainable Development Goal (SDG) No. 7 of the 2030 Agenda aims to "ensure broad access to economical, reliable, and modern energy services", while Target 7.2 aims to "substantially raise the contribution of green energy in the world's energy matrix" [8,9].

The Zambian National Energy Policy of 2019 further acknowledges that because energy is the world's largest commodity market, its resources should be managed sustainably [10]. According to the 2021 World Bank Collection of Indicators, only 46.69% of Zambians had access to power, with urban areas at 85.72% and rural areas at only14.5% [11]. The government's ability to accelerate rural electrification is key to achieving the Vision 2030 Policy's electrification target [12]. Virdy and Yamba state further suggest that the capacity to generate power from low-emission resources and electronic development are crucial for national development [13]. However, the intermittency of renewable resources must be accounted for in hybrid energy systems to ensure uninterrupted power generation.

Approximately 80.5% of Zambia's electricity is derived from hydropower [14]. However, the increasing volatility of rainfall patterns as a consequence of climate change has affected power generation and load shedding, prompting greater dependency on fossil fuels [15,16]. Meanwhile, diesel generators (DGs) are the most common power source in isolated rural areas [17,18]. DGs are associated with fuel cost variability, high operating costs, and environmental impacts from emissions [19]. Therefore, combining DGs with renewable energy (RE) systems is recommended to reduce energy costs and emissions [20,21].

Hybrid renewable energy systems (HRESs) mitigate the impacts of intermittency associated with single renewable energy sources and offer an economically viable solution to dependence on individual resources [22,23]. It is difficult to determine an optimal theoretical design for HRESs, as they are highly site-specific and depend on resource availability, demand, the economic environment, and component costs [24,25]. Battery storage can improve system reliability, balance supply and demand, provide backup power, and reduce fossil fuel consumption [26–30]. Appropriate sizing and configuration of existing commercially available components, however, can be difficult, and, if not adequately addressed, can result in costly and unreliable systems [31–33]. HRES optimization, therefore, requires a comprehensive approach [34–36]. Recent comparative techno-economic studies considering alternative component choices demonstrate the importance of component selection for reliable and economical off-grid HRESs [37,38]. An overview of research on HRES modeling is presented below, organized thematically to reflect principal design decisions faced in off-grid hybrid system planning.

1.1. Optimization Approaches for HRES Sizing and Configuration

Various optimization models have been introduced to test HRES configurations and sizes. Abdulkarim et al. [36] found that the optimal HRES configuration depends on the choice of PV and storage technologies, with observed reductions reaching 90% of Cost of energy (COE) and 73~83% of emissions. Wang et al. [39] demonstrated the benefits of Li-ion batteries by proposing an improved state-of-charge prediction approach. Katti and

Khedkar [40] introduced a component selection method based on the capacity recovery factor, which was adopted by Chauhan and Saini [41] to select optimal wind turbines in isolated Indian villages based on an analysis of the capacity factor. However, PV capacity is typically determined as a continuous variable, while the impacts of PV module ratings, battery technologies, and dispatch strategies are seldom studied in integrated systems, limiting current HRES designs.

1.2. Battery Technology Comparisons

Abdulkarim et al. [36] found that storage technology determines costs and emission standards rather than storage capacity, whereas Biramo [42] established that Li-ion batteries result in comparable COEs as conventional batteries at low ambient temperatures. However, Li-ion batteries are more economical above 25 °C. Khan et al. [43] identified the lead–acid Flow (LAF) battery as the most cost-effective PV/WT/DG system, compared with Li-ion and Vanadium Redox batteries, while Samy et al. [44] found that Nickel–Iron batteries perform better during frequent grid outages. Bhatt et al. [45] demonstrated that second-life Li-ion batteries can reduce system costs by 35% compared with new batteries. On this basis, no single battery chemistry caters to all conditions, as efficacy and cost depend on climate, operation, and system configuration. The role of advances in emerging chemistries, such as lead–carbon batteries, together with dispatch strategies, therefore needs to be better understood [36,45,46].

1.3. Dispatch Strategies and Control Logic

Ramesh and Saini [46] explored the CC, LF, and CD strategies, employing lead–acid and Li-ion batteries in an unelectrified Indian village. They found that the Li-ion-based systems consistently produced the lowest NPC and COE. In another study, Dhavala et al. [17] investigated the LF and PD strategies using lead–acid, Li-ion, and Zinc–bromide batteries in a PV/WT/DG HRES and demonstrated that the Zinc–bromide battery in PD mode was the least expensive alternative. Chaurasia et al. [47] found that a PV/DG/BT installation using a CD strategy lowered COE and associated emissions by 57% and 87% compared to a DG-only system. These papers indicate that the dispatch strategy is an important design variable interacting with battery chemistry.

1.4. Sustainability Assessment

More recently, HRES design has focused on integrating sustainability indicators such as lifecycle emissions, reliability cost, and SDG achievement [9]. The reported emission reductions [36,47] and cost reductions [43,45,46] of HRESs have a range of benefits. However, to date, no full lifecycle assessment has been conducted that includes PV module ratings, battery technology options, dispatch strategy, operational and embodied emissions, and SDG outcomes for unelectrified communities in sub-Saharan Africa.

1.5. Research Gaps and Contributions

Recent studies have also shown that the techno-economic and environmental performance of HRESs depends largely on the types of renewable technologies, battery chemistries, and dispatch strategies adopted, with optimal synergies leading to significantly lower energy costs and emissions while improving reliability. Sustainability considerations in terms of lifecycle impacts and SDG contributions are also increasingly being incorporated into HRES planning. However, the interacting influences of these key design variables are rarely quantified in a holistic manner. In particular, the dynamic effects of combinations of discrete PV module ratings, battery technologies, and dispatch strategies, including burgeoning storage options such as lead–carbon batteries, are infrequently studied within a comprehensive, application-oriented framework. Furthermore, holistic evaluations of

HRESs' techno-economic performance and operational and embodied emissions remain scarce. To address these gaps, this work presents a universal setup for elucidating the interactive effects of combinations of discrete PV module ratings, battery technologies, and dispatch strategies in an off-grid HRES. The novelty of this study lies in integrating discrete PV module ratings, multiple battery chemistries, predictive dispatch strategies, lifecycle carbon assessment, and dual-platform (HOMER Pro–MATLAB/Simulink) validation within a single comprehensive techno-economic evaluation framework for off-grid hybrid renewable energy systems. The net present cost, service life, and frequency of system replacements are used as comparison metrics to model and compare a leading-edge lead–carbon battery using conventional energy storage technologies. In addition to a multidimensional and comprehensive sustainability assessment of operational and lifecycle greenhouse gas emissions, the proposed methodology is validated via two simulation platforms, HOMER ProVersion 3.18 and MATLAB/Simulink Version R2024b, for design guidance. In assessing a hybrid mini-grid for communities without access to modern energy services, impacts on multiple SDGs [48] are also considered. Accordingly, the study contributes not only to methodological advances in HRES evaluation but also to engineering design and evidence-based policy planning by supporting technology selection, rural electrification planning, and investment prioritization for off-grid communities in Zambia and similar Sub-Saharan African contexts.

2. Study Area

The study was conducted in the two un-electrified villages of Bunda Bunda North and Lyamina in the Chinyunyu area of Lusaka Province, approximately 90 km east of the city of Lusaka. Their locations are 15.265791° S, 29.004468° E, and 15.257303° S, 29.017347° E, respectively. Although partly separated by a stream from the Chinyunyu hot spring heritage center, the two villages are part of the same socio-economic catchments and socio-cultural communities. They have similar socio-demographic profiles and are administratively managed as a single community of 535 households (approximately 3210 inhabitants). The villages' economy is based on agriculture (maize, groundnuts, tomatoes, onions, and okra) and livestock (cattle, goats, sheep, chickens, guinea fowls, and pigs). Because there is no grid connection, lighting is mainly provided by candles, battery-powered torches, and small solar lamps, and energy for cooking and heating is derived from firewood and charcoal. Electrification would boost services such as water pumping, healthcare, education, agro-processing, and small-scale enterprises and improve livelihoods.

The research area's geographic location is shown in Figure 1, along with the main entities relevant to the power supply for the designed HRES. Figure 2 shows the annual average solar irradiance of 5.63 kWh/m^2/day, whereas Figure 3 shows the annual average wind velocity of 5.28 m/s. Based on site coordinates, these data were obtained via HOMER from the NASA POWER [49] database, a repository designed for renewable energy and infrastructure modeling that provides near-real-time data [50,51].

The load profile is based on a field survey and served as the basis for load estimation for the study area [52]. It was based on the structure of the households and community facilities, which include a clinic, school, church, police post, roadside shops, and irrigation schemes [53]. Loads were separated into domestic, commercial, community, and agricultural and consisted of various appliances, including lighting, mobile phones, radios, TVs, laptops, refrigerators, fans, electric stoves, office equipment, water pumps, and a milling plant [54]. Because the villages are currently not electrified, there is no historical demand data. As such, the load profile was determined based on ownership and usage patterns obtained through a survey [53]. The load profile therefore illustrates a future demand profile once the system is implemented. This predicted load profile reflects load conditions during

the initial electrification period and inherits uncertainties linked to long-term demand forecasting. As more reliable electricity services become available, ownership demand for productive use and consumption patterns are bound to change, increasing both the absolute magnitude and temporal demand profiles. As such, the optimal HRES configuration identified in this study should be viewed as representative of the initial electrification stage rather than a long-term solution, and periodic re-evaluation of demand and addition of modular system components should be employed to maintain high reliability, low cost, and high-quality services [54]. Table 1 summarizes the load categories, while the daily load profiles for the rainy, cool–dry, and summer seasons are represented graphically in Figure 4.

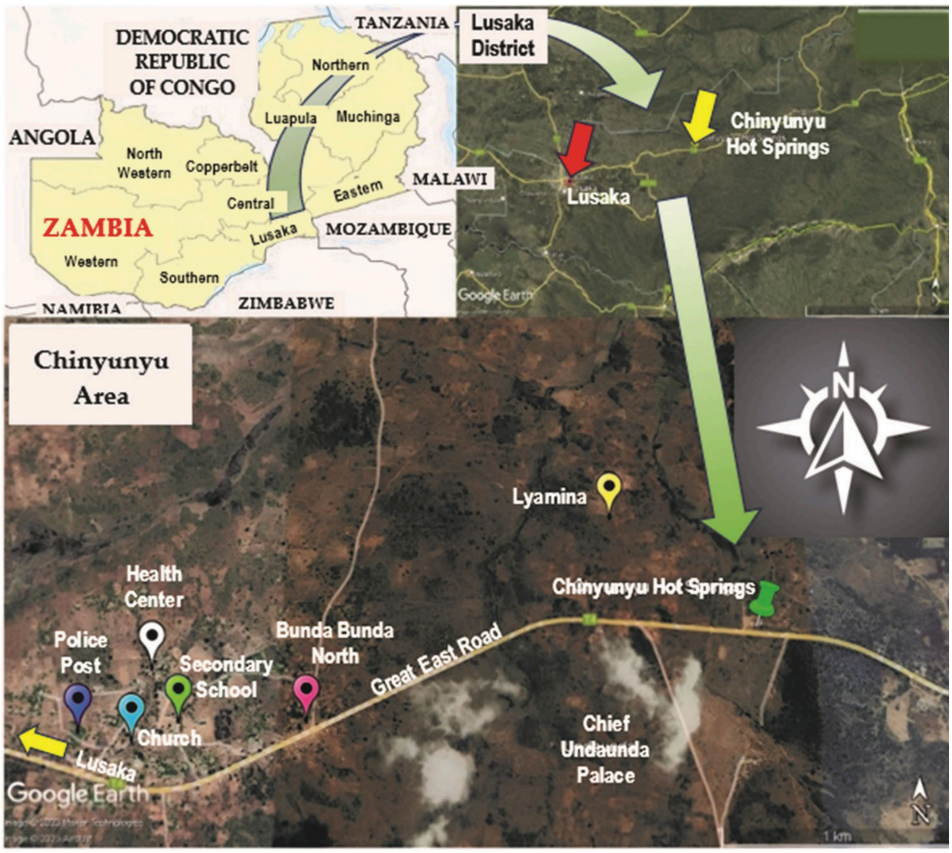

Figure 1. Geographical location of the research site (map obtained with courtesy of Google Earth).

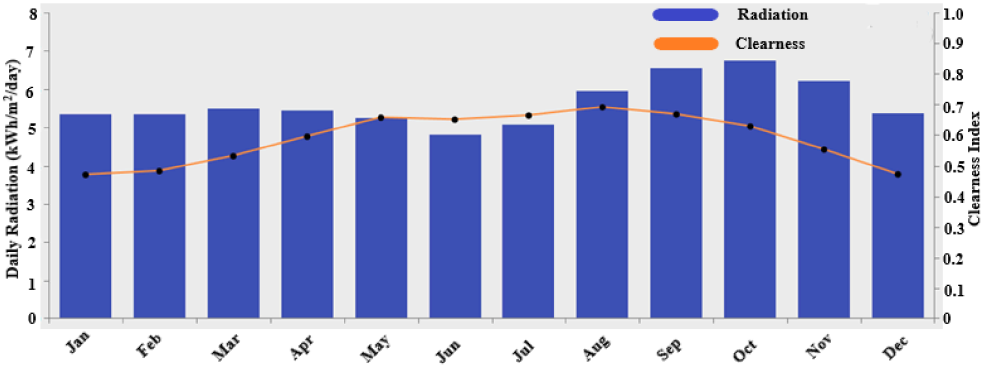

Figure 2. Daily solar radiation and clearness index in the research site.

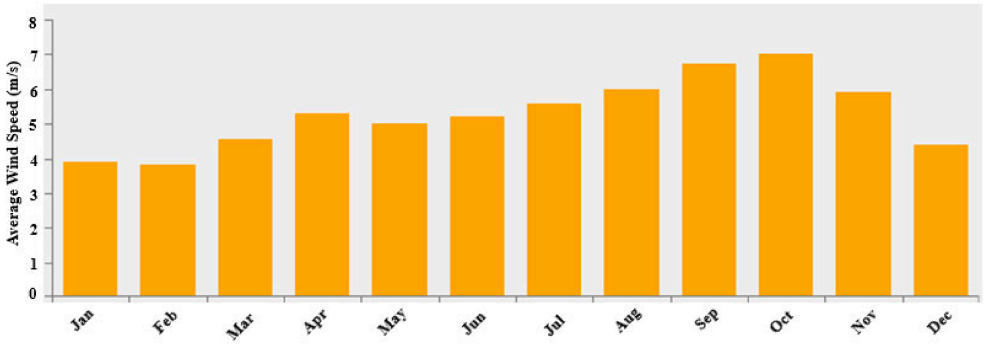

Figure 3. Average wind speed in the research site.

Table 1. Appliance count and power ratings under the different load categories.

		No. of Devices				
Appliance	**Power Rating (W)**	**Domestic**	**Commercial**	**Community**	**Agriculture**	**Total No. of Devices**
60W Bulb	60	1926	65	238	-	2229
TV	150	535	2	8	-	545
Small Fan	75	535	49		-	584
Ceiling Fan	120	-	-	31	-	31
House Refrigerator	120	214	-	-	-	214
Large Refrigerator	200	-	7	14	-	21
Mobile Phone	10	1498	90	65	-	1653
Radio	15	535	45	9	-	589
Laptop	80	214	2	-	-	216
HF Radio	800	-	-	2	-	2
Music System	360	-	2	-	-	2
Electric Stove	2200	-	2	7	-	9
Office Equipment	8940	-	-	1	-	Various
Music Equipment	980	-	-	1	-	Various
Medical Equipment	3470	-	-	1	-	Various
Dental Facility	1200	-	-	1	-	Various
Water Pump	750	-	-	-	24	24
Street Light	300	-	-	30	-	30
Milling Plant	12,500	-	1	-	-	1

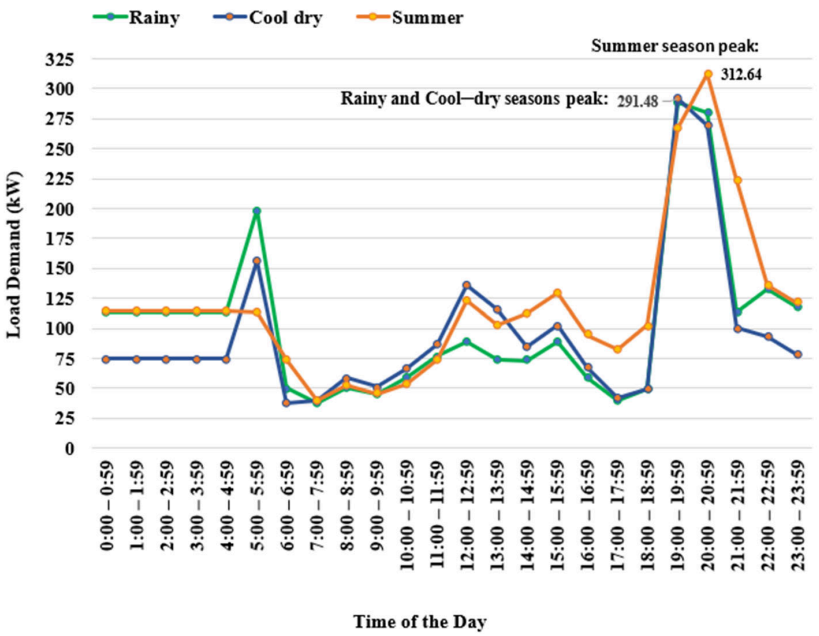

Figure 4. Load curves for rainy, cool–dry, and summer seasons.

Daily loads are estimated using Equation (1) [46].

$$E_{Demand} = \frac{\left(\sum_{i}^{Load} n_{Load-i,j} \times r_{rating-i,j} \times T_{Duration-i,j}\right)}{1000} \quad (1)$$

The daily loads are estimated as 966 kWh/day, 1256 kWh/day, and 1492 kWh/day for the rainy (Dec.–Mar.), cool–dry (Apr.–Aug.), and summer (Sep.–Nov.) seasons, respectively. The daily peak loads are estimated as 312.64 kW for the summer season and approximately 291.48 kW for the cool–dry and rainy seasons.

3. Mathematical Model and Dispatch Strategy for the HRES

Diesel generators are used as a backup supply rather than the main supply for reliability and efficiency. Of the available HRES optimization packages, such as TRNSYS, iHOGA, or HOMER, HOMER Pro Version 3.18 was chosen for its techno-economic optimization of standalone systems [45]. HOMER Pro combines component sizing, optimal dispatch, lifecycle cost analysis, and sensitivity analyses to enable practical comparison of various configurations. While techniques such as mixed-integer linear programming (MILP) 14 and open-source platforms like PyPSA provide greater precision in modeling, they generally demand more comprehensive formulation and analysis tools. A three-step approach was used to determine, simulate, and analyze the techno-economic performance of the HRESs: (i) load and renewable resource estimations; (ii) simulation and optimization of feasible system configurations; and (iii) evaluation of techno-economic results (Figure 5). The component models employed for system simulation are provided and validated using real-world data where available and simulate the most important component operational modes (including efficiencies and losses) for planning-level HRES design.

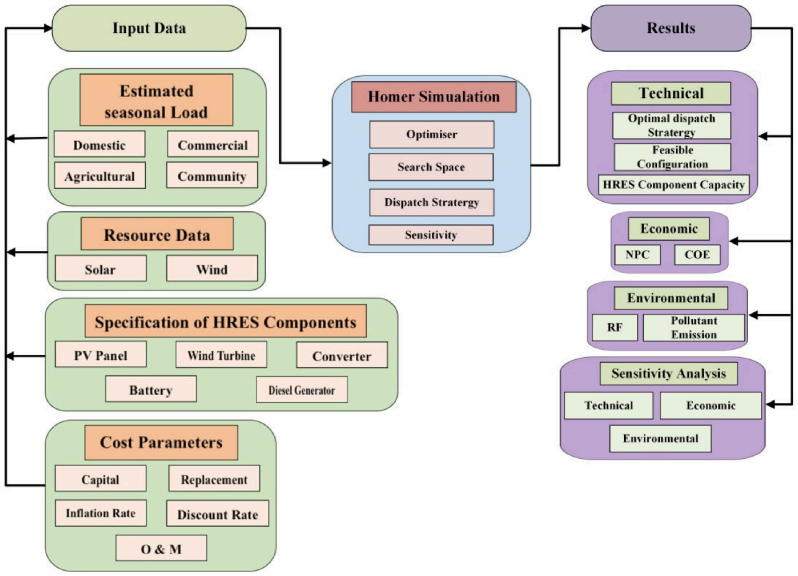

Figure 5. Flowchart showing HOMER simulations and post-HOMER analysis.

3.1. HRES Hardware Modeling

This section presents the simulation of HRES hardware.

3.2. PV System Modeling

The power output from the PV array is determined using Equation (2) [55].

$$P_{PV} = Y_{PV} f_{PV} \left(\frac{G_T}{G_{T,STC}}\right) \left[1 + \alpha_p (T_C - T_{C,STC})\right] \quad (2)$$

Equation (3) provides the energy balance for the PV modules [55].

$$\tau\alpha G_T = \eta_c G_T + U_L(T_c - T_a) \tag{3}$$

Equation (4) can be rearranged to express the PV array's cell temperature, as in Equation (5) [56].

$$T_c = T_a + G_T\left(\frac{\tau\alpha}{U_L}\right)\left(1 - \frac{\eta_c}{\tau\alpha}\right) \tag{4}$$

Given the challenge of obtaining the quantity ($\tau\alpha$/UL) directly, it can be expressed in terms of the Nominal Operating Cell Temperature (NOCT) at an incident radiation of 0.8 kW/m^2 with no load, ambient temperature, and T_a as 20 °C, i.e., η_c as 0. Substituting these values into Equation (4) yields Equation (5), as follows [56]:

$$\frac{\tau\alpha}{U_L} = \frac{T_{c,NOCT} - T_{a,NOCT}}{G_{T,NOCT}} \tag{5}$$

Assuming ($\tau\alpha/U_L$) as a constant ($\tau\alpha$ = 0.9)and substituting Equation (5) into Equation (4) to acquire T_C, as in Equation (6),

$$T_c = T_a + G_t\left(\frac{T_{c,NOCT} - T_{a,NOCT}}{G_{t,NOCT}}\right)\left(1 - \frac{\eta_c}{0.9}\right) \tag{6}$$

Because the quantity $\eta_c/0.9$ is quite small compared to unity, the assumption($\tau\alpha$ = 0.9) does not introduce significant error [56].

Equation (7) is used to estimate the average clearness index in a month [44].

$$K_t = \frac{H_{avg}}{H_{0,avg}} \tag{7}$$

3.3. Wind Turbine Model

HOMER accounts for each time step when calculating wind power. It estimates wind velocity at the turbine hub height in the first phase. The turbine's power output at a specific wind speed and air density is then estimated in the second phase. The power output by a wind system is estimated using Equation (8) [57].

$$P_W = \begin{cases} 0, & V \le V_{Cut-in} and \ge V_{Cut-out} \\ \frac{P_r(V - V_{Cut-in})}{V_r - V_{Cut-in}}, & V_{Cut-in} \le V < V_r \\ P_r, & V_r \le V < V_{Cut-out} \end{cases} \tag{8}$$

Unlike the reference level, the wind speed at hub height (H) depends on the site's location and can be estimated using Equation (9) [58].

$$V = V_{Base}\left(\frac{H}{H_{Base}}\right)^{\alpha_w} \tag{9}$$

3.4. Diesel Generator Model

The DG system acts as a backup power generation unit for the HRES. Equation (10) is applied to estimate the generator's diesel fuel consumption [59].

$$F = (F_{0,DG} \times Y_{DG}) + (F_{1,DG} \times P_{DG}) \tag{10}$$

3.5. Battery Model

The most commonly used storage element in HRESs is the battery, which acts as a backup when RES cannot meet demand [60]. HOMER Pro Version 3.18 uses the kinetic battery model (kbm) to identify battery charging and discharging. The maximum permissible charge and discharge powers of the battery are estimated using Equation (13) [61].

$$P_{Batt,\,Cmax} = \frac{min\left(P_{Batt,Cmax,kbm} P_{Batt,Cmax,mcr} P_{Batt,Cmax,mcc}\right)}{\eta_{Batt,C}} \tag{11}$$

where $\eta_{Batt,c}$ = efficiency of charge storage.

$$P_{Batt,\,Cmax,kbm} = \frac{kQ_1 e^{-k\Delta t} + Qkc\left(1 - e^{-k\Delta t}\right)}{1 - e^{-k\Delta t} + c\left(k\Delta t - 1 + e^{-k\Delta t}\right)} \tag{12}$$

Equation (13) gives storage charge power at the maximum charge rate.

$$P_{Batt,Cmax,mcr} = \frac{\left(1 - e^{-\alpha_c \Delta t}\right)(Q_{max} - Q)}{\Delta t} \tag{13}$$

Equation (14) gives the maximum charge current corresponding to storage charge power.

$$P_{Batt,Cmax,mcc} = \frac{N_{Batt} \times I_{max} \times V_{nom}}{1000} \tag{14}$$

Functional battery degradation is modeled as a gradual decrease in storage capacity. Degradation due to temperature is determined from Equation (15) [56]:

$$k_t = Be^{-d/T} \tag{15}$$

The number of cycles to failure varies inversely with the DoD. HOMER Pro Version 3.18 uses the Rain flow Counting algorithm to convert the battery's state-of-charge time series into discrete cycles, each with a specific DoD. The fraction of lifetime degradation for each cycle is then calculated, and cumulative degradation is determined using Equation (16) [56]:

$$DoD = \sum_{i=0}^{N_C} A(DoD)^{\beta} \tag{16}$$

HOMER Pro Version 3.18 simulates battery lifetime using a throughput-based wear mechanism. It tracks the annual energy cycled (in kWh) against the manufacturer's lifetime throughput limit, which is based on capacity, efficiency, and chemistry. Once the cumulative throughput reaches this limit, the battery is depleted. HOMER then schedules a replacement and adds the cost to the net present cost (NPC), determining the total number of replacements needed over the 25-year project.

3.6. Converter Model

The converter is appropriately sized to ensure a reliable connection between the AC and DC buses, facilitating bi-directional power conversion [62]. The main functions of the bi-directional converter are to sustain the power flow in the HRES and to act as a power conditioning device. The converter's efficiency is determined by taking the ratio of the input and output power using Equation (17), as described by [46]. The converter size in this study is taken as 10% greater than the peak load.

$$\eta_{in} = \frac{P_o}{P_{in}} \tag{17}$$

3.7. Economic Modeling

The economic parameters used to estimate the feasibility of the designed HRES are the COE and the net present cost (NPC).

3.8. Cost of Energy (COE)

The cost of energy is calculated using Equation (18) [46]:

$$COE = \frac{Cann, tot}{E_{Served}} \tag{18}$$

where

$$C_{ann,tot} = CRF\left(i, R_{Proj}\right) C_{NPC} \tag{19}$$

where

$$CRF = \frac{i(1+i)^N}{(1+i)^N - 1} \tag{20}$$

3.9. Net Present Cost (NPC)

HOMER Pro Version 3.18 uses the NPC to represent the lifecycle cost [63]. The NPC of the HRES is determined by subtracting the present value of the system's revenue over the project's lifetime from the present value of all capital, operating, and maintenance expenditures [46].

3.10. HRES Hardware Input Parameters

This study considered three types of solar PV panels rated at 335 W, 400 W, and 445 W, one wind turbine rated at 1 kW, three types and ratings of batteries (100 Ah-LA, 200 Ah-LC, and 100 Ah-Li-ion), and a converter rated at 344 kW. Selection was based on practical availability in the local market, compatibility with other system components, and capacity to offer an optimal trade-off between performance and cost. Considering a wider range of PV panel ratings would have significantly increased computational complexity without yielding proportionate improvements in results. The selected ratings align with industry standards and the existing literature on HRES design. The decision variables, constraints, and assumptions for this study in HOMER Pro Version 3.18 are given in Table 2. The technical and cost parameters of the main components utilized as inputs in HOMER Pro Version 3.18are presented in Table 3a,b. The economic evaluation focuses on primary cost factors such as capital cost, replacement cost, O&M cost, fuel cost, and discount rate. The cost components were derived from local market research and vendor information to create an authentic regional economic scenario.

Table 2. Decision variables, constraints, and assumptions used in HOMER simulation.

HRES Component	Decision Variables	HOMER Built-In Key Constraints/Assumptions	Verification
PV	Rated capacity (kW)	Linear scaling with irradiance + derating; MPPT (ideal)	MATLAB Simulink (924 kW match)
Battery (Li-ion)	Battery size (kWh)	SOC limits, round-trip efficiency, throughput-based lifetime model	Not fully verified in this study
DG	Rated capacity (kW)	Minimum load ratio, operating reserve, fuel curve	HOMER internal dispatch
Dispatch Strategy	PD strategy	Internal controller logic	PD strategy selected in HOMER
Objective Function	-	Minimize NPC	NPC = USD 3,856,895 COE = USD 0.151/kWh

Table 3. (**a**) Technical input specifications of the HRES. (**b**) HRES economic input specifications.

(**a**)

Component	Model	Manufacturer	Rating	Voltage (V)	Efficiency (%)	Lifetime (Years)	Notes
Solar PV	AS-335	Dayliff	335 W	12	15	25	Derating: 88% Ground reflection: 88%
	YL-400M	Dayliff	400 W	12	15	25	Derating: 88%
	STPXXXS-B72/Pnh+	Suntech	445 W	12	20.4	25	Ground reflection: 88%
Wind Turbine	HY-CI10-48-AWMMT	HY Energy	1 kW	48	Not Specified	20	Hub height: 17 m
Diesel Generator	HOMER auto-sized	Kirloskar	350 kW	415	Not Specified	60,000 hours	Fuel: diesel Fuel cost: USD 1.30/L
Battery—Lead–Acid	4R-1040TC	Dayliff	1.2 kWh	12	85	5	Max capacity: 100 Ah
Battery—Lead–Carbon	NP-100-12 L	RENTECH	2.63 kWh	12	85	15	Max capacity: 200 Ah
Battery—Lithium-Ion	JPC 12-200	WECO	5.2 kWh	48	99	15	Max capacity: 100 Ah
Converter	Generic	Generic	344 kW	Conceptual	95	15	Rectifier eff.: 95%

(**b**)

Component	Capital Cost (USD/kW)	Replacement Cost (USD/kW)	O&M Cost (USD/kW per y)
Solar PV	883	490	8.83
	997	554	9.97
	728	404	7.28
Wind Turbine	13,377/unit	8360/unit	133/unit per y
Diesel Generator	516	287	0.030/op.h
Battery—Lead–Acid	1092 (set of 4)	840 (set of 4)	1.09 (set of 4/y)
Battery—Lead–Carbon	2527 (set of 4)	1944 (set of 4)	2.53 (set of 4/y)
Battery—Lithium-Ion	3275/unit	2519/unit	3.30/unit per y
Converter	301	188	3.01

Note: Capital costs cover local delivery and installation labor but exclude VAT and excise duties in accordance with Zambian law. Technical performance data are based on manufacturer information [64–68], whereas labor and transport prices have been adjusted to 2025 Lusaka Province market conditions [69]. *Capital costs:* PV Panels and diesel generator = 180% of Cost; wind turbine and inverter = 160% of cost; Battery = 130% of Cost. *O&M costs:* PV Panels, WT, inverter, and DG = 1% of cost; Battery = 0.1% of cost. *Replacement Costs:* Taken same as the initial Component costs.

The HRES PV/WT/DG/BT/converter combination is given in Figure 6. The DG connects to the AC bus, and the PV, WT, and battery connect to the DC bus. The converter is coupled with both the DC and AC buses.

3.11. Dispatch Strategies

When power from Renewable Energy Sources (RES) cannot meet load demands, a well-planned dispatch strategy is essential to optimize the overall performance of a HRES. These rule-based strategies govern interactions among the RES, battery storage, and diesel generators (DGs). This work considers four built-in HOMER Pro Version 3.18 dispatch strategies described as follows: [17,46]:

- *Load Following (LF)*: The DG operates strictly to meet the immediate load deficit and does not charge the batteries ($P_{DG} = P_{load} - P_{RES}$). Instead, battery charging takes precedence only when excess renewable energy is available.
- *Cycle Charging (CC)*: Whenever the DG is activated to meet load demands, it operates at its maximum nominal capacity ($P_{DG} = P_{rated}$). Any surplus power generated beyond the immediate load requirement is used to charge the batteries.
- *Combined Dispatch (CD)*: This hybrid approach balances cost and efficiency by alternating between the LF and CC strategies based on immediate demand, rather than projecting future needs. It employs the CC strategy during low-load periods to efficiently charge batteries and switches to the LF strategy during peak loads.
- *Predictive Dispatch (PD)*: Unlike the other methods, PD forecasts upcoming power demand and renewable resource availability (such as solar radiation and wind speed) to optimize battery utilization and further reduce HRES operating costs.

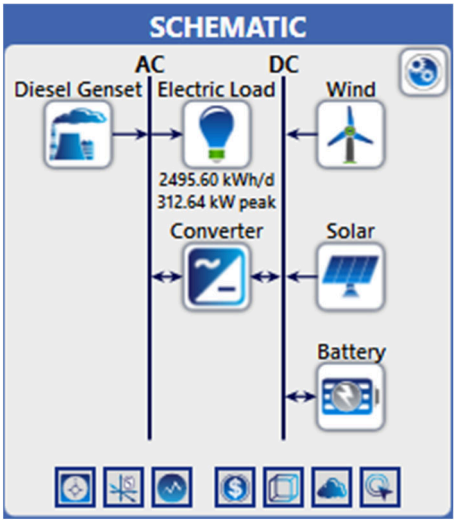

Figure 6. Schematic diagram of the simulated HRES.

The PD strategy manages diesel generator (DG) operation and battery State of Charge (SoC) based on a 48h forecast of load demand and renewable energy generation. It activates when the forecasted renewable output and current battery SoC are insufficient to meet upcoming demand. To minimize fuel consumption and operating costs, the PD method strategically discharges the batteries before renewable resources become available. By creating "empty capacity" in the battery bank early, the system ensures that it can recharge using upcoming clean energy (such as solar and wind) rather than relying on expensive, less environmentally friendly DG power. The success of this approach depends heavily on accurate forecasting and adequate battery capacity. Ultimately, all the rule-based strategies described above are tested within the simulation framework to compare their impact on system performance and cost.

By prioritizing renewable energy over the DG, the PD method decreases fuel consumption, lowers operating costs, reduces emissions, and prevents surplus renewable energy from being wasted. While preemptively discharging batteries might raise concerns about shortened lifespan due to frequent deep discharges, the PD strategy is actually designed to protect battery health. It strictly maintains the SoC above the minimum limit (SoC_{Min}) to prevent damaging deep discharges. Additionally, by forecasting energy availability, the system optimizes its charge and discharge cycles, reducing wear from unnecessary cycling. The strategy also mitigates battery aging by avoiding prolonged periods at a high SoC;

discharging ahead of predicted renewable generation prevents extended overcharging, ultimately improving battery longevity.

While HOMER suggests dispatch strategies and outlines their general structure, it does not provide a specific method for their implementation. Although Predictive Dispatch is implemented using HOMER Pro's built-in dispatch strategy, the software does not explicitly describe its operational sequence. Therefore, Figure 7 presents a conceptual control logic developed by the authors to illustrate how the HOMER Predictive Dispatch strategy was represented and interpreted for the present study. The flowchart is intended to explain the operational decision sequence and does not replace or modify HOMER's internal optimization algorithm.

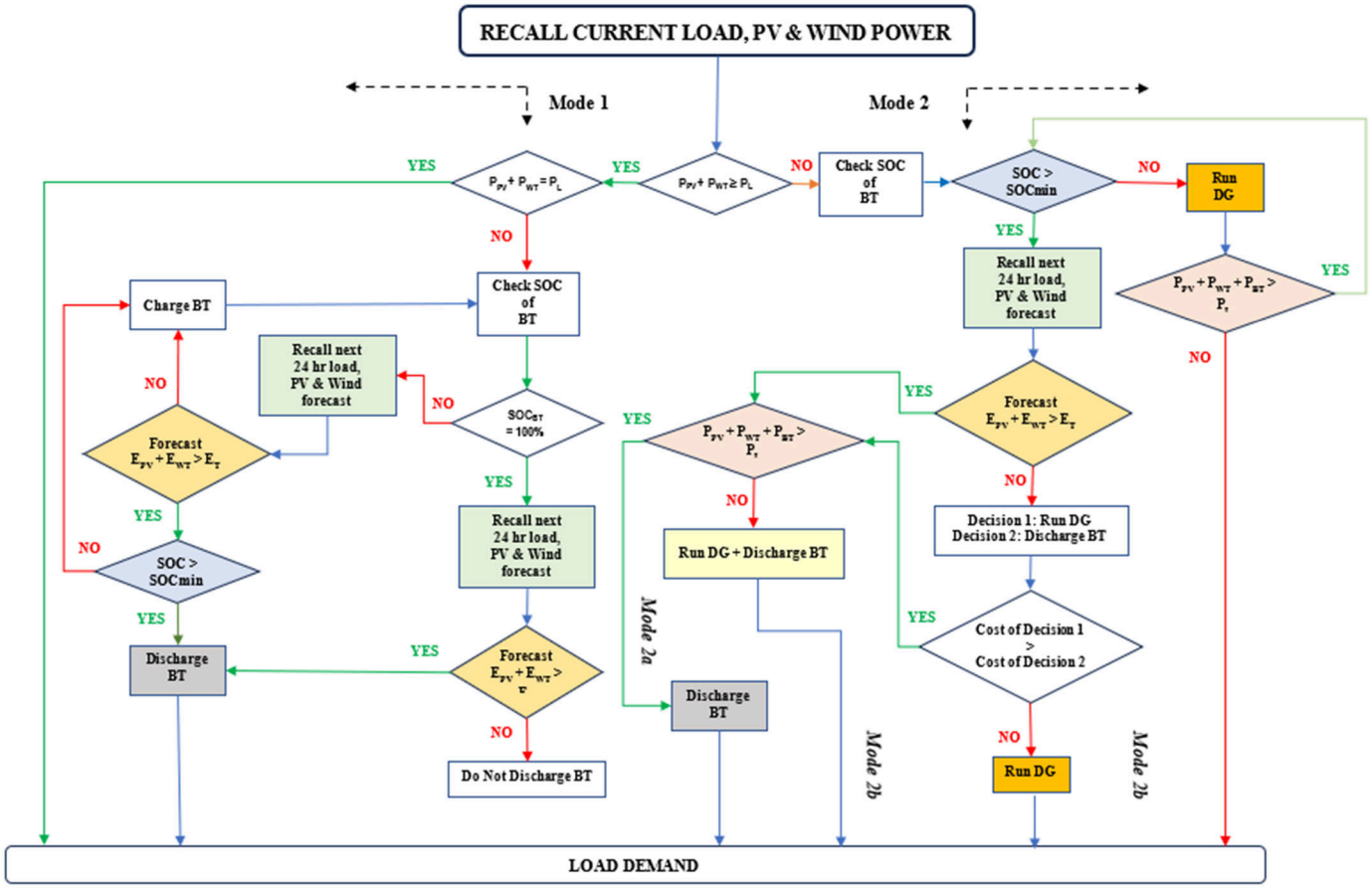

Figure 7. Conceptual control logic of the PD strategy.

Mode 1: When $P_{PV} + P_{WT} \geq P_L$

In Mode 1, the load is primarily fulfilled by the RES, i.e., $P_{PV} + P_{WT} = P_L$. If the load is not fulfilled by the RES, i.e., $P_{PV} + P_{WT} < P_L$, then the battery's SOC is first checked. If the SoC is 100%, forecasting for PV and wind is conducted to verify whether these sources can meet the expected load in 24 h. If the forecasted energy from solar and wind is found to exceed the total energy requirement, i.e., $E_{PV} + E_{WT} > E_T$, the battery will be allowed to discharge. If the total forecasted load from solar and wind falls below the load requirement, then the battery will not be allowed to discharge.

Mode 2: When $P_{PV} + P_{WT} \leq P_L$

In this mode, when the generated power from solar and wind is lower than the required load, i.e., $P_{PV} + P_{WT} < P_L$, the system first checks the SoC of the battery, and the following two sub-modes arise.

Mode 2a: Battery SoC > SoC_{min}

When the battery SoC exceeds the minimum threshold ($SoC > SoC_{min}$), the system initiates a 24h energy forecasting process to estimate the availability of power from solar and wind systems. The objective is to determine whether upcoming renewable energy generation will be sufficient to provide the expected power, P_L. If forecasted power from PV and wind exceeds the total power for the forecast horizon, the system verifies whether the combined power ($P_{PV} + P_{WT} + P_{Battery}$) surpasses the immediate demand, P_L. If this is the case, the system will strategically use the battery by discharging it to fulfill the power demand.

However, if the predicted energy from PV and wind is less than the total energy demand for the next 24 h, the system checks whether DG power generation is necessary. Nevertheless, prior to starting the DG, the system considers the expense of running the DG to decide whether it is cheaper to rely on stored battery energy or turn on the DG. If operating the DG is more expensive or unnecessary, the battery is discharged to supply the demand, and the DG is only engaged afterward, lowering fuel consumption and operational costs. This method guarantees that renewable energy is used to the fullest while optimizing system performance and minimizing reliance on fossil fuels.

Mode 2b: Battery SoC $\leq SoC_{min}$

If $SoC \leq SoC_{min}$, the DG is turned on, and the condition $P_{PV} + P_{WT} + P_{Battery} > P_L$ is verified. If not, the demand is entirely supplied by the DG. However, if the condition is met, the condition $SoC > SoC_{min}$ is checked, and 24h energy from solar and wind is forecast. If the forecasted PV and wind energy are expected to exceed the total demand, the system follows the path of Mode 2a, discharging the battery.

However, if the forecasted energy from solar and wind is expected to be less than the total energy demand, the system considers two possible options, i.e., running the DG or discharging the battery. The costs of both options are assessed, and, if running the DG is more economical, the system selects this option. Otherwise, the system checks whether $P_{PV} + P_{WT} + P_{Battery} > P_L$. If it is not satisfied, the load demand is met by using a combination of the DG and the battery.

The forecast values for the predictive dispatch rules are extracted directly from the deterministic synthetic hourly time series imported into HOMER Pro 3.18without using any external forecasting modules (e.g., NASA, ECMWF, or MATLAB). The 48h load forecasts in the community load profile are derived from appliance-level field surveys shown in Table 1 and Figure 4, while the 24h PV and wind forecasts (for Mode-2a/2b) are derived from the same hourly irradiance and hub height wind speed data used for the site's energy balance calculations shown in Figures 2 and 3. Because the controller reads exact future simulation values, the PD strategy operates with perfect foresight over the 24h and 48h windows without modeling forecast uncertainty. Consequently, SoC deviations are expected to stem from parameters such as component efficiencies, ramp limits, minimum SoC, and seasonal load. This enables external validation using software such as MATLAB/Simulink, as the custom controller can be replicated exactly. Due to this lack of an error buffer, the output parameters represent upper-bound achievable values. Robustness to climate variability is evaluated by directly altering the solar and wind input data, rather than introducing a stochastic forecasting model into the controller. This method aligns with the deterministic look-ahead approach established earlier. Ultimately, it demonstrates that the advantage of the PD strategy is based on its ability to handle resource fluctuations, rather than relying on the accuracy of short-term weather predictions.

However, there is a symmetric operation for forecast deviations. If the actual 48h load exceeds the forecast, the planned battery pre-discharge drains faster than expected, causing the battery to hit SoC_{min} earlier than anticipated and forcing the diesel generator to engage sooner than simulated. Conversely, if renewable generation exceeds forecasts or the load

is lower than expected, the controller's pre-discharge decisions are overly conservative. The battery can absorb the surplus, but the altered charge/discharge schedule still impacts cycling-related battery degradation.

For the post-HOMER simulation, four cases are selected for analysis: (i) diesel generator (DG) only as the base case, (ii) PV/DG/BT, (iii) PV/WT/DG/BT, and (iv) PV/BT. The optimized results for these cases are shown in Tables A1 and A3.

3.12. Operational Emission Assessment

HOMER calculates the emissions resulting from running the diesel generator based on a total of six emissions comprising GHGs, CO_2, and five air pollutants: CO, UHC, PM, SO_2, and NO_x. It calculates the emission factor, which represents the amount of pollution released for each unit of fuel used. The emissions are then estimated by multiplying by annual fuel consumption [56].

3.13. Lifecycle Carbon Emission Assessment

To complement the operational emissions analysis, a basic lifecycle assessment (LCA) was performed to estimate the total carbon emissions of the DG-only system and the HRES configurations. The analysis adopts a cradle-to-grave lifecycle perspective over a 25-year project lifetime, considering component manufacturing (embodied emissions), transportation, operation, and end-of-life processes. However, to ensure a conservative and unbiased comparison among technologies, only the manufacturing, transportation, and operational stages were included in the quantitative lifecycle emission calculations, while end-of-life processes were considered qualitatively and are discussed separately below. The functional unit is defined as 1 kWh of electricity supplied to the load.

Emission factors for major system components were obtained from the literature and are summarized in Table 4. The embodied emissions of PV modules, batteries, wind turbines, diesel generators, and converters were estimated by multiplying installed capacities by their respective emission factors. Operational emissions for the diesel generator were obtained directly from HOMER Pro Version 3.18 simulation outputs, while operational emissions for renewable components were assumed to be negligible. Transportation emissions were estimated based on component weights and assumed transport distances of 10,000 km by sea (and 1000 km by road) using standard emission factors per ton-kilometer. The number of replacements was determined based on the component lifetimes relative to the 25-year project lifetime summarized in Table 5.

The total lifecycle emissions, E_{total}, were calculated using Equation (21) [70]:

$$E_{total} = E_{embodied} + E_{transport} + E_{operation} \quad (21)$$

Battery replacement over the project's lifetime was implicitly included in the emission estimates. The resulting emissions were aggregated over the 25-year project period and compared across dispatch strategies and system configurations.

Although a cradle-to-grave perspective was adopted, end-of-life emissions were intentionally excluded from the quantitative calculations because recycling credits (e.g., for lead or aluminium) can produce negative emission values that may bias comparisons in favour of certain technologies. Excluding these credits therefore provides a more conservative and consistent basis for comparing the carbon footprints of the alternative system configurations.

Table 4. Assumed emission factors and parameters used for the lifecycle assessment.

Item	Adopted Unit Mass Value	Adopted Emissions Value	References
PV modules (embodied)	70 kg/kW	600 kg CO_2/kW	[65,71,72]
Diesel generator (embodied)	15 kg/kW	400 kg CO_2/kW	[68,73]
Wind turbine (embodied)	70 kg/kW	0.026 kg CO_2/kWh	[68,74]
Li-ion battery (embodied)	10 kg/kW	150 kg CO_2/kWh	[66,75]
Converter (embodied)	10 kg/kW	100 kg CO_2/kW	[74]
PV operational emissions	-	0.04 kg CO_2/kWh	[76]
Wind operational emissions	-	0.013 kg CO_2/kWh	[77]
Diesel operational emissions	-	From HOMER	HOMER Pro software
Transport (sea)	-	0.01 kg/ton-km	[78]
Transport (road)	-	0.15 kg/ton-km	[78]
Sea distance	-	10,000 km	-
Road distance	-	1000 km	-
Project lifetime	-	25 years	-

Table 5. Number of component replacements over the project's lifetime.

Component	No. of Replacements
PV panel	0
Wind turbine	1 (at year 20)
Lead–acid batteries	4 (at years 5, 10, 15, and 20)
Lead–carbon batteries	1 (at year 15)
Li-ion battery	1 (at year 15)
Diesel generator	0 (based on simulated run times over the project's lifetime)
Converter	1 (at year 15)

4. Results and Discussion

The proposed PV/WT/DG/BT HRES is evaluated against an integral sustainability index (technical, economic, environmental, and social aspects) focused on reliable and affordable low-carbon electrification to meet the SDGs. A techno-economic analysis is carried out under the conditions of three PV modules (335 W, 400 W, 445 W), three battery technologies (lead–acid, lead–carbon, and Li-ion), and four dispatch strategies (LF, CC, CD, PD). The feasible candidate systems are PV/WT/DG/BT, PV/DG/BT, and PV/BT, while the system with DG only is used as a baseline. DG only has an NPC of USD 14,101,860 and a COE of USD 0.5523/kWh for comparison.

4.1. Performance Analysis of Different Ratings of PV Panels

For HRES performance analysis, simulations were conducted using three PV panel ratings (335 W, 400 W, and 445 W), three battery types, and four dispatch strategies. Performance is based on NPC and COE, as shown in Figure 8a–f. The highest NPC values were observed using the LC battery under the CC strategy. The 400 W PV panel yielded the highest NPC, while the 335 W panel exhibited a slightly lower NPC across all strategies

and battery types. In contrast, the 445 W panel consistently yielded the most cost-effective NPC and COE because this panel has a 38% lower cost (USD 1.64/W) than the 335 W panel (USD 2.64/W) and a 34% lower cost than the 400 W panel (USD 2.49/W), as shown in Table 3a,b. In addition, the comparatively higher conversion efficiency of 20.4% means more energy is generated per unit area. Because the component and O&M costs are assumed to be fixed fractions of the capital cost, these costs per watt propagate linearly into the lifecycle cost. Furthermore, fewer modules (11% and 33% fewer than the 400 W and 335 W panels, respectively) are approximated with the associated system hardware, resulting in a lower balance-of-system cost component. Increased energy generation over the HRES's lifespan also reduces the cost per unit of energy. Thus, NPC (including mounting structures, wiring installation labor, and land footprint) is minimized. Under the CC strategy with the LC battery, Case-3, using the 400 W PV panel, had an NPC 34% higher than the base case, while the 335 W panel resulted in a 32% increase and the 445 W panel led to a 31% increase. Conversely, using a Li-ion battery under the PD strategy in Case-2, the NPC was approximately 70% lower than the base case for the 400 W PV panel, 71% lower for the 335 W panel, and73% lower for the 445 W panel, minimizing lifecycle cost. It also maximizes energy output, making the 445 W solar panel particularly effective and warranting further study. For these reasons, further analysis is conducted with the 445 W solar panel-based HRES.

To analyze the system's power exchange performance, a period from the power output curves is typically selected for each configuration [79]. Figures 9–12 illustrate the power output curves for a typical week from 29 August to 4 September for different configurations. Figure 9 represents the base case, in which the DG meets the load demand, resulting in high operating costs (NPC and COE) and significant pollution. In the PV/WT/DG/BT-based HRES, shown in Figure 9, the wind system contributes a negligible load of approximately 2 kW.

Figures 10–12 show that during the daytime, electricity demand is predominantly met by solar power, which also charges the battery bank. During the night, the battery, wind turbine, and DG collectively meet the load, with the battery bank meeting most of it. Simultaneously, the DG activates only during the early morning hours, when solar radiation and the clearness index are low, and the battery's SoC falls below a specific limit. Figures 10 and 11 also show that although the PV and battery primarily met the load for most of the week, on 3 September, the DG was prompted to run with maximum efficiency to provide steady generation to concurrently provide the load and recharge the battery due to low solar radiation and a reduced clearness index experienced on2 September, which caused the battery's SoC to fall below its lower limit. This behavior emphasizes the interdependence between solar variability, battery storage dynamics, and dispatch control strategies. Reduced solar generation will cause batteries to be discharged more deeply, increasing reliance on diesel generators and ultimately leading to higher fuel consumption, operational costs, and overall system expenditure.

4.2. Effect of LF, CC, CD, and PD Strategies on HRES Performance

Table 6 presents the optimized results for the three selected configurations, PV/WT/DG/BT (Case-1), PV/DG/BT (Case-2), and PV/BT (Case-3), under the PD strategy. For further comparison, the same parameters are presented for the LF, CC, and CD strategies in Table A1. The PV/DG/BT (Case-2) configuration is the most feasible, giving an NPC of USD 3,856,895 and a COE of USD 0.151/kWh. In contrast to the base case, the NPC for Case-1 (PV/WT/DG/BT) is 72% lower, and that for Case-2 (PV/DG/BT) is 73% lower. These cases result in a significant cost reduction compared to the base case. When com-

paring Case-1 and Case-2 directly, the difference in NPC is only 1%, which nonetheless remains significant when considering the additional factors involved.

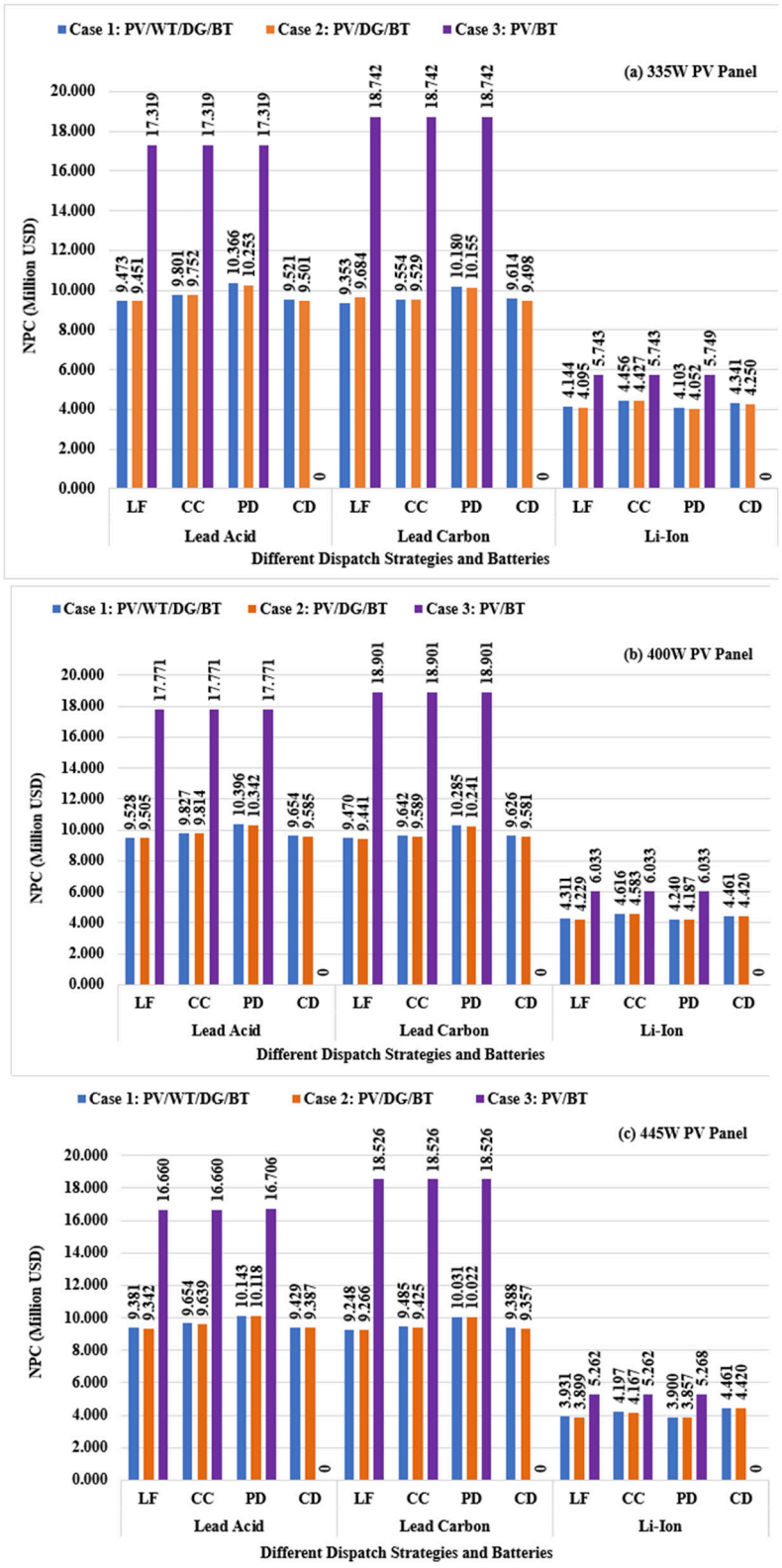

Figure 8. *Cont.*

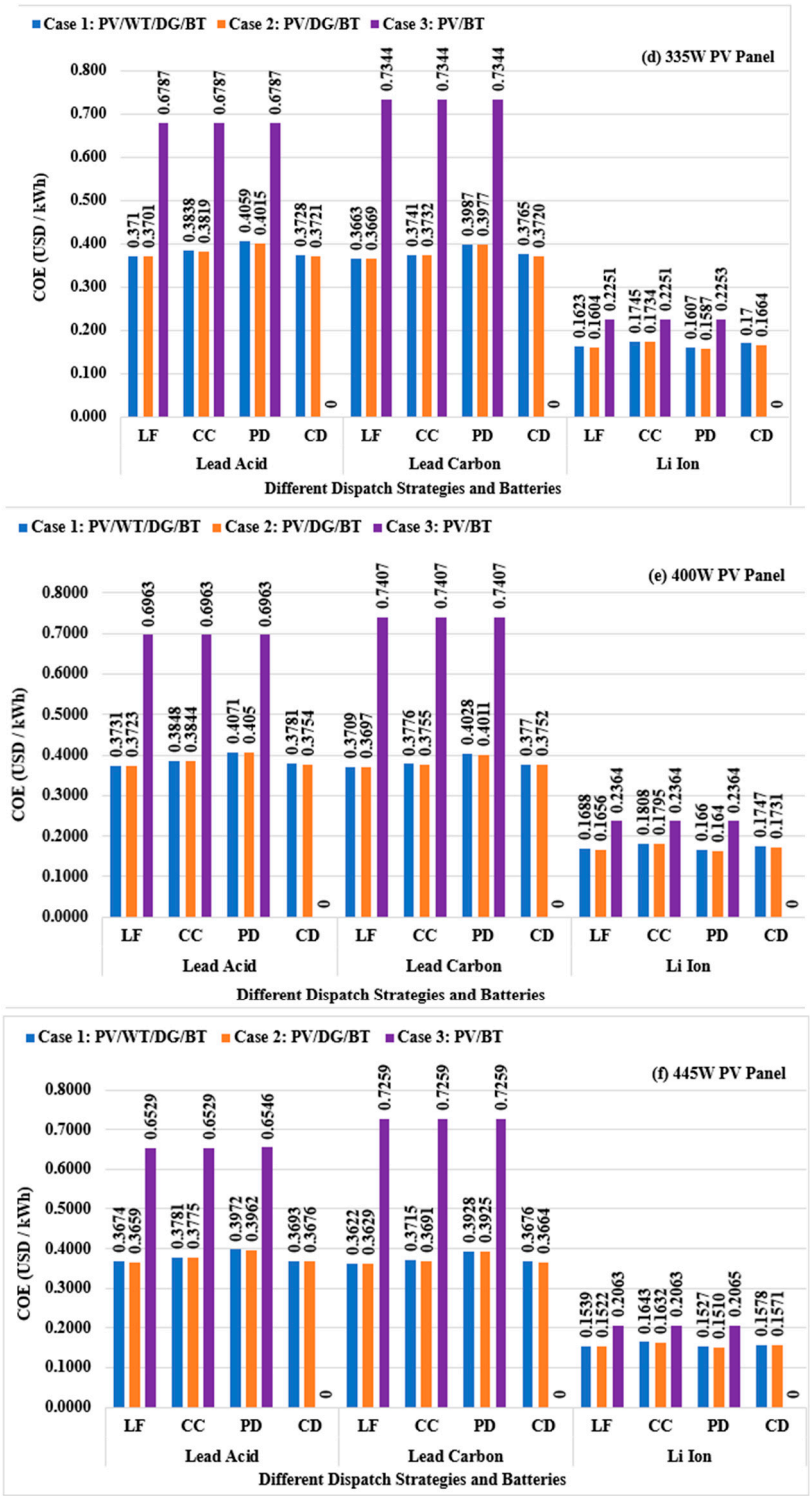

Figure 8. NPC and COE for the proposed HRES using different ratings of PV panels, batteries, and dispatch strategies. (**a**) NPC with regard to the 335 W PV panel; (**b**) NPC with regard to the 400 W PV panel (**c**) NPC with regard to the 445 W PV panel (**d**) COE with regard to the 335 W PV panel (**e**) COE with regard to the 400 W PV panel (**f**) COE with regard to the 335 W PV panel.

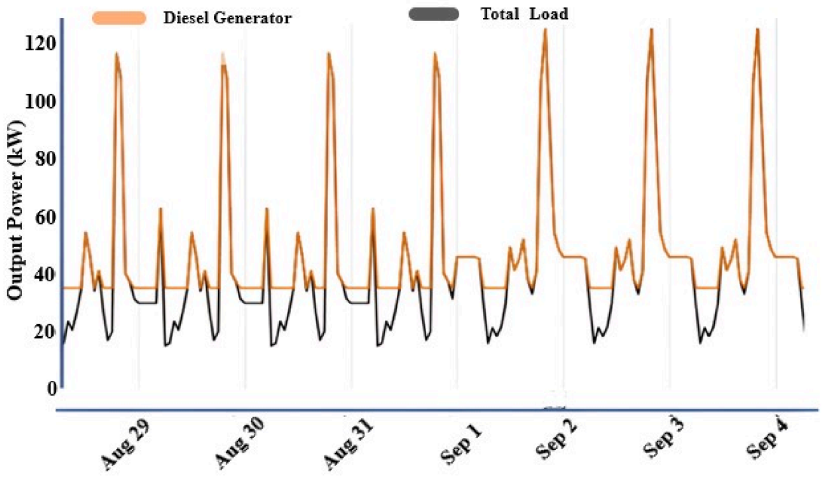

Figure 9. Output power curve for the base case (DG only) from 29 August to 4 September.

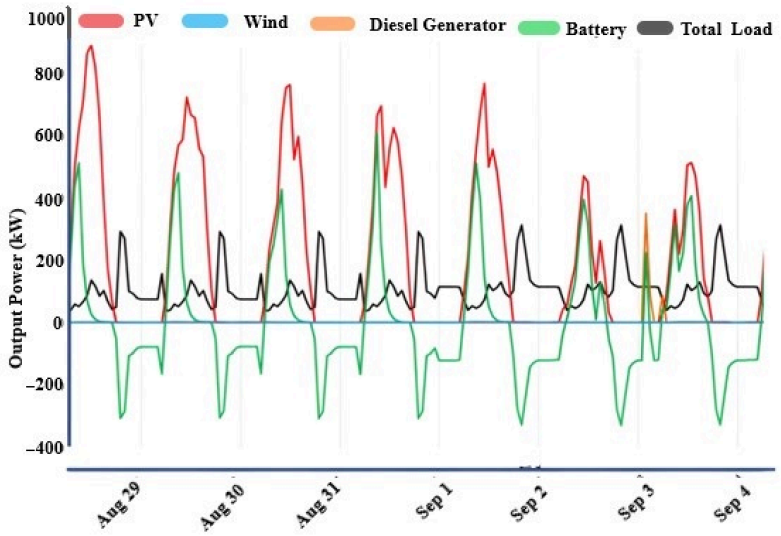

Figure 10. Output power curve for the PV/WT/DG/BT HRES from 29 August to 4 September.

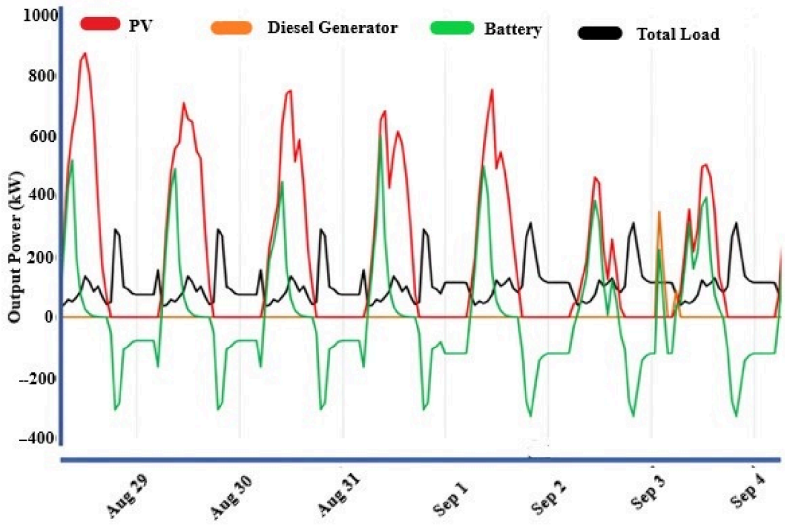

Figure 11. Output power curve for the PV/DG/BTHRES from 29 August to 4 September.

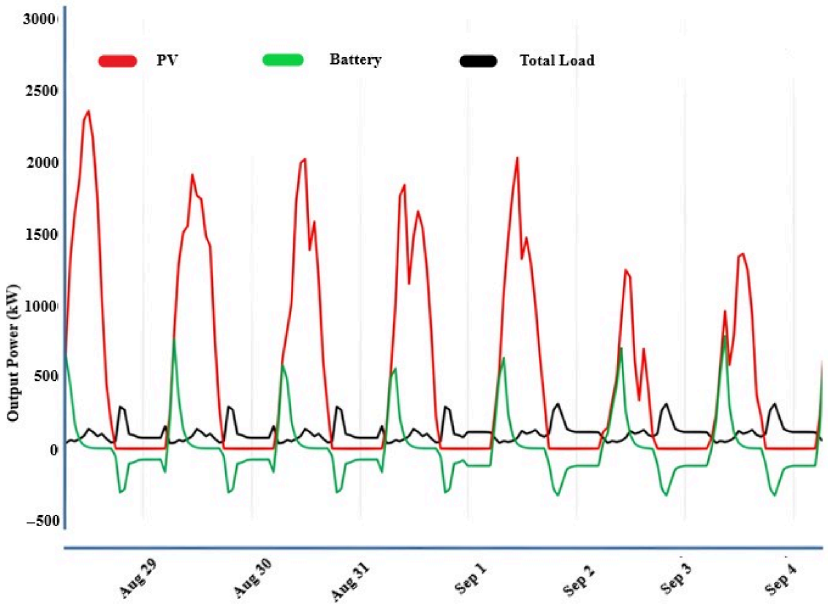

Figure 12. Output power curve for the PV/BT HRES from 29 August to 4 September.

Table 6. Optimized results of the Li-ion battery-based HRES under the PD strategy.

Battery Type	**Li-Ion**		
Case No	1	2	3
PV (kW)	938	924	2484
Wind (Nos)	2	-	-
DG (kW)	350	350	-
Battery (Nos.)	444	439	534
Converter (kW)	344	344	344

Case-1 leverages wind energy as an additional renewable input. However, it simultaneously increases system complexity and requires higher-level system management. As such, the small economic gain of Case-2, along with simpler operational control, less intermittency, and lower maintenance, make it more practical. Although the two setups differ by only 1% in NPC, Case-2 is more practical, as it strikes a favorable balance between cost and operational feasibility while still reducing NPC by 73%. Conversely, the NPC and COE values for the PV/BT (Case-3) configuration are higher than those of the base case, rendering it the least favorable option.

An evaluation of the three selected configurations of the proposed HRES using the three types of batteries shows that the highest NPC and COE values occur with the LC battery, whereas the Li-ion battery yields the lowest NPC and COE, making it the most feasible choice. Among the four dispatch strategies, the CD strategy yields the highest values, while the PD strategy yields the most cost-effective NPC and COE. Compared to the base case, the NPC is approximately 69% lower under the CD strategy, 70% lower under the CC strategy, and 72% lower under the LF strategy. The greatest reduction is observed under the PD strategy, giving an NPC 73% lower than the base case. The PD strategy can achieve the lowest NPC by intelligently planning energy flows by forecasting power demand and renewable generation. It reduces reliance on diesel generator operation and prevents excessive battery cycling. CC and CD strategies often run the diesel generator for extended periods or under sub-optimal load conditions, leading to higher fuel consumption and increased operational costs. Moreover, these approaches can cause the battery to be charged

and discharged more deeply or more frequently, accelerating battery degradation and increasing replacement costs over the system's lifetime. Among the four, the LF strategy performs better than the CC and CD approaches by reducing unnecessary generator operation; however, it lacks predictive capability, limiting its ability to minimize lifecycle costs. The outstanding economic results of the PD strategy can be attributed to its lower fuel consumption, reduced battery stress, and enhanced overall system efficiency. A comparable pattern is observed in COE values across these strategies, further confirming that the PD strategy is the most cost-effective. Table 3 presents detailed comparative results for the three selected cases, PV/WT/DG/BT (Case-1), PV/DG/BT (Case-2), and PV/BT (Case-3), concerning the445 W-based HRES utilizing three different batteries under four dispatch strategies.

4.3. Impact of Batteries on Performance of HRES

Maintaining battery SoC within the recommended thresholds is critical when designing HRESs with battery storage [58]. To evaluate the proposed HRES, three types of batteries, i.e., LA, LC, and Li-ion, were considered. The LA and LC batteries are designed to discharge to 20% SoC, while the Li-ion batteries are designed to discharge to 10% SoC or lower [46]. The SoC for these batteries during the chosen week, 29 August to 4 September, is shown in Figures 13–15. The figures reveal that the LA battery discharges to nearly 20% and the Li-ion battery to approximately 10%, while the LC battery does not reach its 20% discharge limit during the week, remaining at around 60% SoC. This indicates that the DoD for Li-ion batteries is significantly higher than that of LA and LC batteries. While manufacturers specify the DoD limits for these batteries during the design phase, this demonstrates the advantage of Li-ion batteries over their counterparts in approaching their maximum DoD. Their larger capacity provides a greater power supply, reducing the frequency of charging and discharging cycles. It also requires fewer batteries to meet the same load demand, reducing system complexity and NPC. These advantages render the Li-ion battery a reliable and more cost-effective option for the HRES under study.

The results show that the maximum NPC and COE are associated with the LC batteries, while the Li-ion batteries offer the most optimal economic performance. Among the three configurations, Case-2 provides the lowest costs. In contrast to the base case, the NPC is reduced by approximately 28% and 29% with LA and LC batteries. However, the Li-ion batteries achieve a significant NPC reduction of approximately 73%. Figure 16 illustrates the Li-ion battery's SoC for a typical year, during the month of September, and on 5 September. From December to March, the batteries discharge to their designed limit of 10% due to low solar radiation from the low clearness index during the rainy season. The relatively low charging rate, along with the higher demand for lighting during these months, further intensifies discharge. From April to August, the batteries discharge to approximately 35% due to a relatively higher clearness index and lower load demand during the cool, dry season. In contrast, during the summer months of September to November, the batteries discharge to their 10% limit. This is because greater use of indoor fans increases power demand, despite the higher clearness index during these months, which allows for higher PV generation.

Table A2 presents further details on the performance of the three configurations using LA, LC, and Li-ion batteries under the PD strategy, while Table 7 presents Battery performance under the PD strategy. The results indicate that Li-ion batteries provide a higher usable nominal capacity, greater lifetime throughput, and increased annual throughput compared to the other battery types. Additionally, in all cases, the Li-ion batteries exhibit significantly lower losses than both the LA and LC batteries.

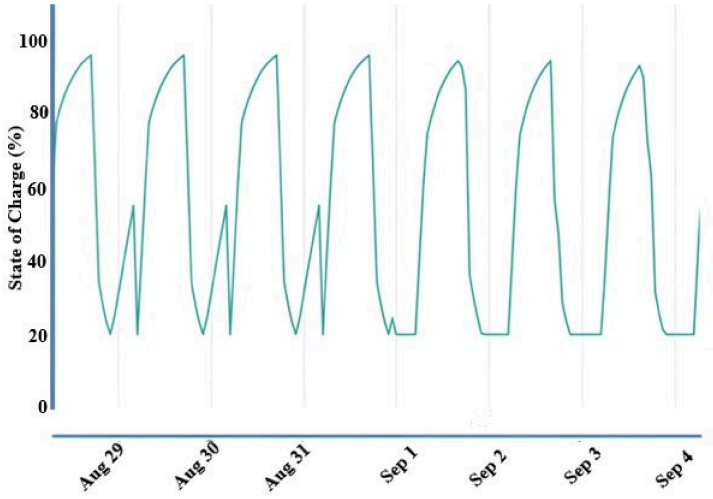

Figure 13. SoC of LA battery in a typical week.

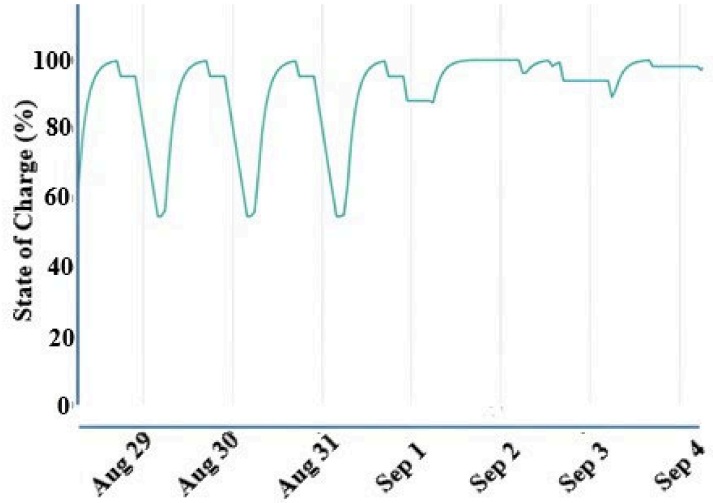

Figure 14. SoC of LC battery in a typical week.

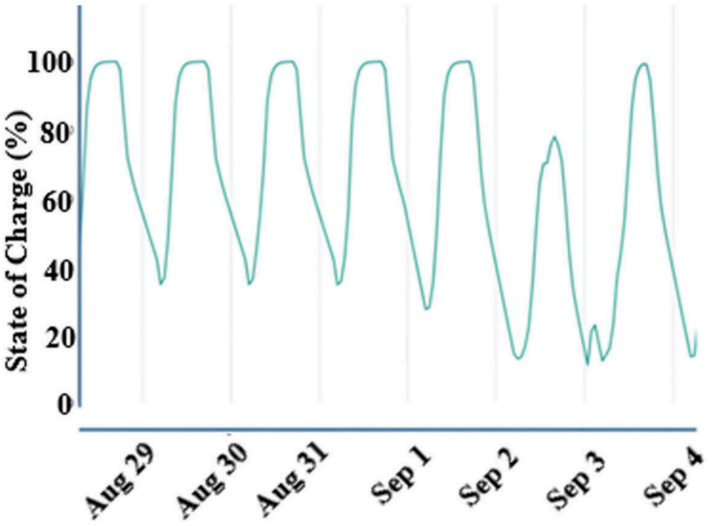

Figure 15. SoC of Li-ion battery in a typical week.

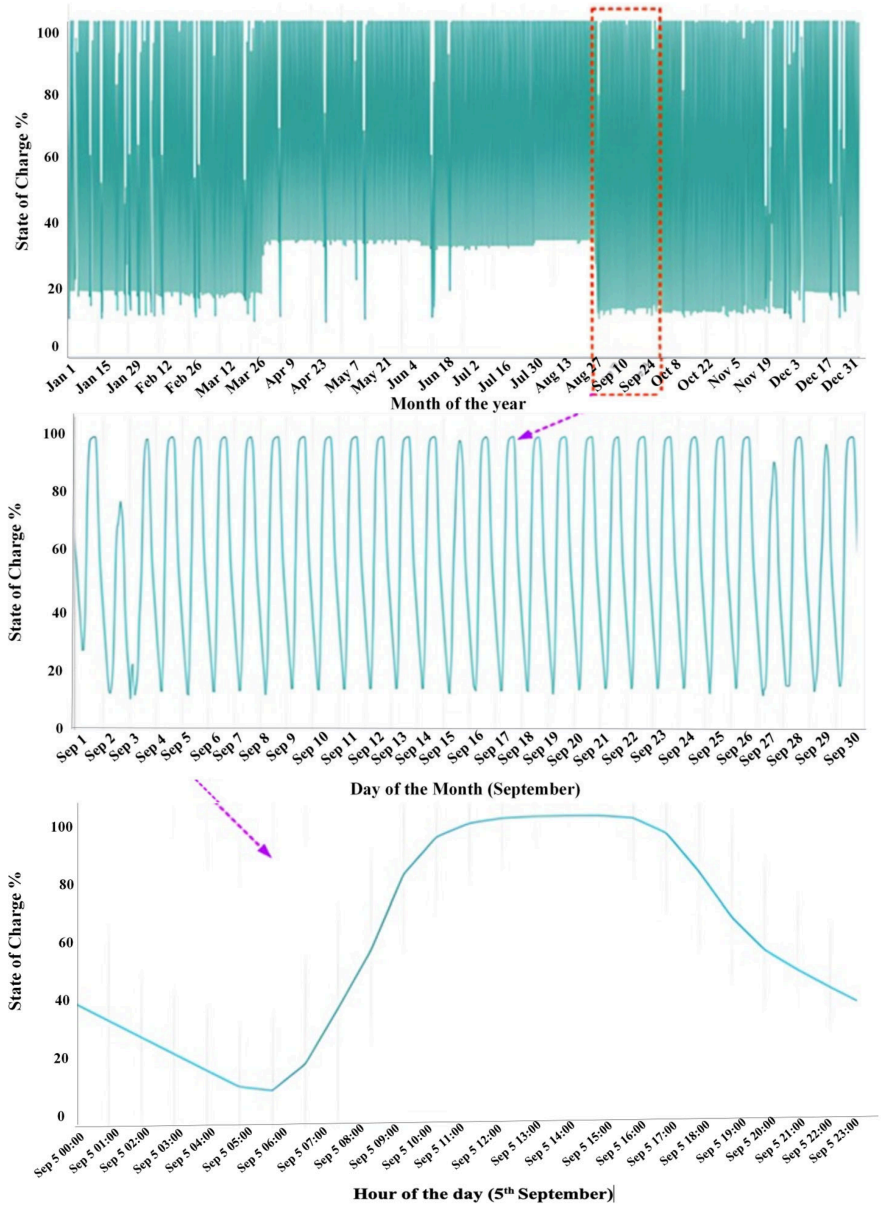

Figure 16. Typical daily, monthly, and annual SoC of the Li-ion battery.

Lithium-ion batteries, with their higher depth of discharge, draw on a higher percentage of stored energy without increasing the battery bank's capacity. In addition, because they last much longer, fewer replacements over the lifecycle result in less NPC. Their greater efficiency, on the other hand, means that energy is lost less often, which is beneficial for the generation requirement. In comparison, lead–acid and lead–carbon batteries are far more prone to degradation, especially when subjected to repeated deep discharge cycles and elevated temperatures [80]. These conditions catalyze processes such as sulfation and electrolyte degradation, which together reduce the battery's capacity, shorten its lifespan, and increase replacement frequency. Due to their temperature sensitivity, lead–acid batteries perform even worse at high ambient temperatures, whereas Li-ion batteries remain fairly stable. This makes the latter less prone to temperature swings, making them a better fit for reliable, cost-effective operation even in tropical climates.

Table 7. Li-ion Battery performance under the PD strategy.

	Case No.		
Parameter	**Case-1**	**Case-2**	**Case-3**
Nominal Capacity (kWh)	2309	2283	2777
Nominal Capacity (Nos.)	444	439	534
Usable Nominal Capacity (kWh)	2078	2055	2499
Lifetime Throughput (kWh)	9,267,268	9,292,427	9,452,132
Expected Life (y)	15	15	15
Energy in (kWh/y)	620,925	622,544	632,303
Energy out (kWh/y)	614,721	616,324	626,983
Losses (kWh/y)	3900	3943	3551
Annual Throughput (kWh/y)	617,818	619,428	630,142

4.4. Impacts of Dispatch Strategies on Pollutant and Lifecycle Emissions

A thorough comparison of CO_2 and pollutant emissions under various dispatch techniques between the optimal HRES and the DG-only system is shown in Table A3, while Table 8 presents the Operational CO_2 and pollutant emissions of the DG-only and HRES under the PD strategy. Pollutants are drastically decreased across all strategies compared with the base case, and using the DG alone for electrification results in annual CO_2 emissions of approximately 793,467 kg/y, while other pollutant emissions amount to 5002 kg/y of CO, 218 kg/y of UHC, 30.3 kg/y of PM, 1943 kg/yr of SO_2, and 4698 kg/y of NOx. These pollutants contribute to environmental degradation and health issues. However, adopting an HRES significantly reduces CO_2 emissions. Depending on the dispatch strategy used, emissions from the HRES range from 2.5% to 3.8% of those from the DG system, making them nearly negligible. Consequently, transitioning from a DG-only system to an HRES for power supply in the study area substantially lowers GHG and pollutant emissions.

Table 8. Operational CO_2 and pollutant emissions of the DG-only and HRES under the PD strategy.

	Base Case	**PD Strategy**	
Emissions (kg/y)	**DG Only**	**Case-1**	**Case-2**
CO_2	793,467	28,225	30,291
CO	5002	178	191
UHC	218	7.76	8.33
PM	30.3	1.08	1.16
SO_2	1943	69.1	74.2
NOx	4698	167	179

Because emissions vary with the chosen dispatch strategy, selecting an appropriate strategy is essential. Among the four strategies, the PD strategy yields the highest total emissions at 28,648 kg/y for Case-1 and 30,745 kg/y for Case-2.

In contrast, the LF strategy yields the lowest total emissions at 20,140 kg/y in Case-1 and 24,240 kg/y in Case-2. Compared to the base case, pollutant emissions are significantly reduced by 96.1% and 96.4% under the PD strategy and by 96.9% and 97.5% under the LF strategy. This comparison shows that the difference in emissions between the LF and PD strategies is approximately 1%. Because optimizing NPC and COE is the study's main goal,

the HRES under the PD method is recommended despite its slightly higher emissions, as it better aligns with the optimization objectives.

A lifecycle emissions analysis of the DG-based HRES with a Li-ion battery was conducted, accounting for embodied, transportation, and operational emissions over the 25-year lifetime of the plant, as summarized in Table 9.

Table 9. Lifecycle CO_2 emissions for DG-only and HRES configurations under different dispatch strategies.

System	Strategy	Total Embodied (kg CO_2)	Total Transport (kg CO_2)	Total Operational (kg CO_2)	Total LCA Emissions (kg CO_2)
DG Only	—	140,000	1313	19,836,675	19,977,988
Case-1	LF	1,152,641	26,254	497,151	1,676,047
Case-2	LF	1,144,848	25,678	598,067	1,768,592
Case-1	CC	1,337,519	31,159	679,304	2,047,982
Case-2	CC	1,340,305	31,163	616,826	1,988,294
Case-1	CD	1,244,901	28,599	681,063	1,954,564
Case-2	CD	1,247,228	28,653	685,918	1,961,798
Case-1	PD	1,099,987	24,382	706,564	1,830,934
Case-2	PD	1,087,420	24,050	758,199	1,869,669

The DG-only system produces the highest emissions, totaling approximately 19.98 million kg CO_2, with emissions driven almost entirely by operational fuel consumption. In contrast, all HRES configurations significantly reduce total lifecycle emissions, with values ranging from approximately 1.68 to 2.05 million kg CO_2, corresponding to reductions of approximately 90–92% relative to the DG-only system. Among the dispatch strategies, the load following (LF) strategy achieves the lowest emissions, followed closely by the predictive dispatch (PD) strategy, with only marginal differences (less than 1%) between them.

A key observation is the shift in emission structure between system configurations. While the DG-only system is dominated by operational emissions, the HRES configurations are primarily influenced by embodied emissions, particularly from PV modules and battery storage systems. Transportation emissions, although included, account for a minimal fraction of total emissions across all configurations.

These findings highlight an important trade-off in hybrid renewable energy systems: reducing long-term operational emissions comes at the cost of increased upfront embodied emissions. Nevertheless, even when all lifecycle stages are considered, the HRES configurations remain significantly cleaner than the DG-only system throughout the project's lifetime, confirming net environmental benefits when assessed from a whole-life perspective.

4.5. Validation and Verification of Results

A two-stage validation procedure was adopted. In the first stage, the PV subsystem model results from HOMER Pro Version 3.18 are recreated in MATLAB/Simulink Version R2024b under identical operating conditions (solar irradiance, temperature, PV panel rating, and load conditions) and compared with PV power production [24]. The close agreement between HOMER Pro Version 3.18 and MATLAB/Simulink Version R2024b confirms the accuracy of the PV subsystem model; however, it should not be interpreted as validation of the complete hybrid energy system. In the second stage, the NPCs and COEs are compared against those of other HRESs in Table 10 which show good agreement in both magnitude and trend. The close agreement between HOMER Pro and MATLAB/Simulink confirms the accuracy of the PV subsystem model; however, it should not be interpreted as validation of the complete hybrid energy system. Consequently, the results should be interpreted as planning-level estimates.

MATLAB/Simulink Version R2024b modeling was used to simulate the operation and performance of the optimized HRES, focusing on technical efficiency and investigating several scenarios to validate the results obtained with HOMER Pro Version 3.18 [24]. Figures 17–20 show the I-V curve and P-V curves of the PV model. As shown in Tables A1 and 6, under the PD strategy and with Li-ion batteries in Case-2 (PV/DG/BT), the PV panel's output power is 924 kW. When the same system was independently run in the MATLAB/Simulink Version R2024b model, the simulated PV panel power output was also 924 kW, confirming the accuracy of the HOMER Pro Version R3.18 results.

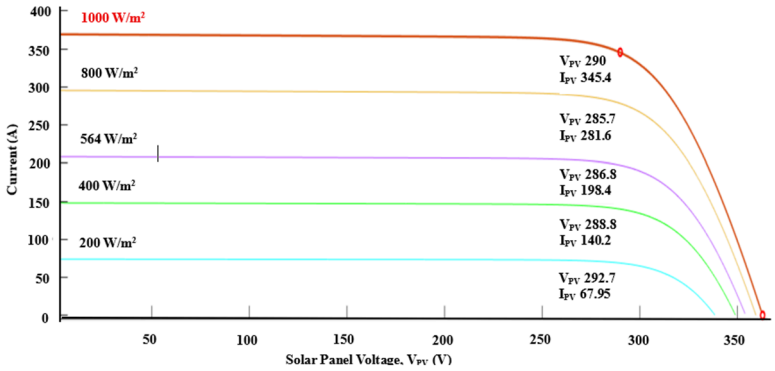

Figure 17. I-V curve of the 445 W PV panel obtained from MATLAB Simulink.

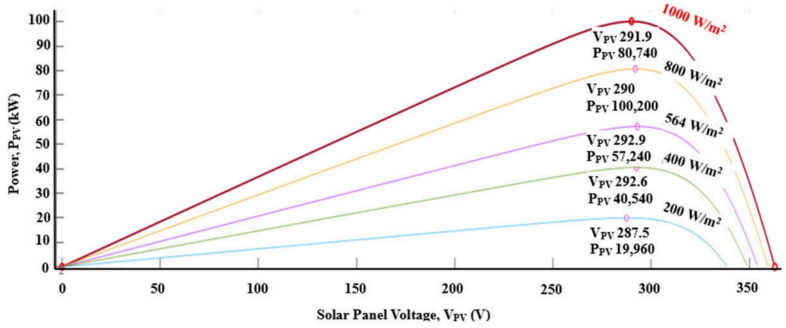

Figure 18. P-V curve of the 445 W PV panel obtained from MATLAB Simulink.

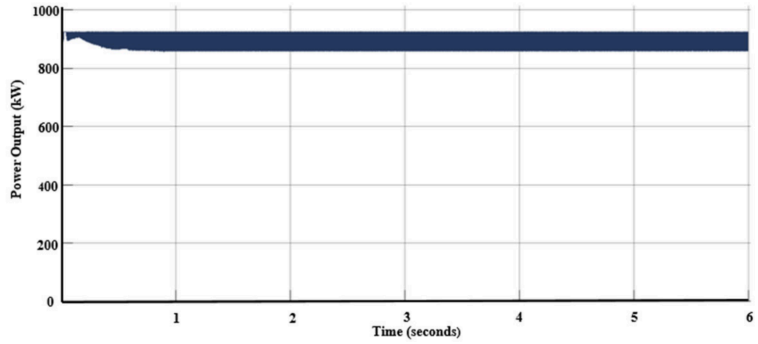

Figure 19. Power output of 445 W PV panel obtained from MATLAB Simulink.

Because the Chinyunyu site cannot be field-verified, the COE of the optimal PV/DG/BT system, USD 0.151/kWh, was benchmarked against similar HOMER studies, confirming its techno-economic competitiveness, as shown in Table 10. However, practical affordability remains a challenge for low-income rural households. The COE is significantly higher than ZESCO's USD 0.0175/kWh lifeline tariff but below the USD 0.40/kWh–USD 0.57/kWh range recommended for sustainable Zambian mini-grids [7]. To bridge the

gap between affordable pricing and cost-reflective tariffs, financial sustainability requires strong policy support and strategic cost-recovery mechanisms such as tiered tariffs, pay-as-you-go (PAYG) models, and cross-subsidization [81–83]. Crucially, prioritizing demand aggregation and productive loads, such as the identified 12.5 kW milling and 18 kW irrigation loads, will generate the higher revenues needed to subsidize residential users and ensure the project's long-term scaling. This multidimensional balance will be vital to enable sustainable scaling of decentralized systems in a rural developing context, where divergence between affordable energy prices and cost-reflective tariffs can often hinder project scaling [54,84,85].

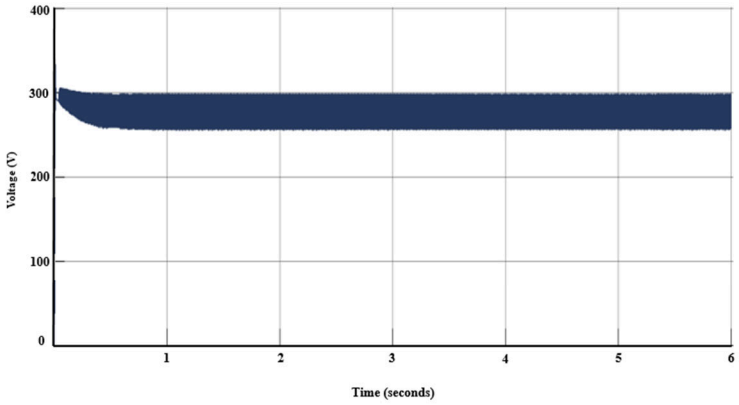

Figure 20. Voltage output of 445 W PV panel obtained from MATLAB Simulink.

Table 10. Comparison of present study and similar studies conducted in Zambia and internationally.

Authors	HRES Configurations Investigated	Region and Peak Load	Technique/Tool	Battery Type and Dispatch Strategy	Objective Function	Findings
Present Work	PV/WT/DG/BT PV/DG/BT PV/BT	Chinyunyu, Zambia, 312.6 kW	HOMER	BT: LA, LC, Li-ion DS: LF, CC, CD, PD	NPC = USD 3,856,895 COE = USD 0.151/kWh	The PV/DG/BT is optimal when using larger PV panels along with the Li-ion battery under the PD strategy.
[86]	PV/DG/BG/BT	Enugu State, Nigeria, 104.1 kW	HOMER	BT: Li-ion DS: Not Stated	NPC = USD 303,312 COE = USD 0.066/kWh	Increasing the proportion of biogas in the HRES eventually eliminates the need for DG, lowering the NPC and COE.
[87]	DG/Grid, PV/DG/Grid PV/BG/Grid PV/WT/BG/Grid BG/Grid, PV/BT/Grid	Blantyre, Malawi, 23.7 kW	HOMER	BT:Not Stated DS:Not Stated	NPC = USD 79,511 COE = USD 0.095/kWh	The PV/BG/Grid system is the most optimal. The addition of DG increases NPC values, while the inclusion of batteries increases operating costs due to their short lifespan.
[7]	PV/BT	Various locations in Zambia, 24.4–51.8 kW	End-use model, basic financial equations	BT:Not Stated DS: Not Stated	COE = USD 0.4/kWh–USD 0.57/kWh	In rural locations, PV mini-grids are typically not financially feasible and may require some type of subsidy.
[88]	PV/BG/BT	Mbeya, Tanzania 63.41 kW	HOMER, GWO	BT:Li-ion DS: Not Stated	NPC = USD 106,383.50 COE = USD 0.1109/kWh NPC = USD 85,106, COE = USD 0.0887/kWh	Application of the GWO technique decreases financial metrics.

Table 10. *Cont.*

Authors	HRES Configurations Investigated	Region and Peak Load	Technique/Tool	Battery Type and Dispatch Strategy	Objective Function	Findings
[89]	PV/WT/BG/BT/HT WT/BG/BT/HT PV/BG/BT/HT	Linze, China, 134.6	HOMER	BT:Li-ion DS: LF, CC	NPC = USD 1,260,000 COE = USD 0.162/kWh	The PV/WT/BG/BT/HT combination is most suitable. However, as the H_2 load increases, the NPC and COE also increase.
[90]	PV/WT/BT	Jamataka, Botswana, 27.31 kW	HOMER	BT: LA DS: Not Stated	NPC = USD 339,804 COE = USD 0.298/kWh	During the HRES design phase, battery systems' capacity and O&M expenses must be carefully taken into account.
[17]	PV/WT/DG/BT PV/BT	Karnataka, India, 37.34 kW	HOMER	BT:LA, Li-ion, ZB DS:LF, PD	NPC = USD 55,262 COE = USD 0.35/kWh	The PV/WT/DG/BT combination with a zinc–bromide battery under the PD strategy is optimal.
[91]	PV/BM/BT	El Santuario, Honduras, 8 kW Mumbezi, Zambia, 0.5 kW	HOMER	BT:Not Stated DS: Not Stated	NPC = USD 256,133 COE = USD 0.06/kWh NPC = USD 564,697, COE = USD 0.48/kWh	The technical and economic aspects of an islanded PV–biomass hybrid microgrid are viable compared to grid extension in both cases.
[46]	PV/WT/MH/DG/BT PV/MH/BT	Karnataka, India, 108.63 kW	HOMER	BT:LA, Li-ion DS: LF, CC, CD	NPC = USD 465,790–USD 716,658 COE = USD 0.1/kWh–USD 0.162/kWh	The PV/MH/BT system under the LF strategy is optimal using a Li-ion battery.
[92]	PV/WT/DG/BT	Eastern Cape, South Africa, 54.34	HOMER	BT:Li-ion DS: LF, CC, CD, PD	COE = USD 0.1382/kWh	The PD strategy is most feasible.

4.6. Sensitivity Study

A rigorous sensitivity analysis is carried out to examine the deviations in input variables that affect the system, such as discount rate, battery cost, PV cost, fuel cost, load demand, solar irradiation, ambient temperature, and battery life. The analysis is centered on the PV/DG/BT HRES with a Li-ion battery under the PD strategy, as it offers the most cost-effective NPC and COEs.

4.6.1. Impact on NPC Due to Input Variables

Figure 21 shows how a 20% change in input parameters affects the NPC. The results indicate direct proportionality between NPC and changes in PV, battery, and fuel costs. In addition, a 20% change in fuel costs results in the smallest NPC fluctuation of approximately 1–2%. Regarding PV cost, a 20% change causes a minor increase in NPC variation of around 2–5%, whereas a 20% change in battery cost has a significantly greater impact on NPC, resulting in changes of approximately 5–12%. The significant effect of battery cost changes is likely because the PD mode focuses more on batteries to meet the load rather than the DG, reducing fuel consumption. Furthermore, lower PV cost fluctuations are due to the irregular nature of solar energy. Meanwhile, NPC has an inverse relationship with the discount rate; a 20% change in the discount rate leads to an NPC change of approximately 6.5%. This inverse relationship results from the fact that the discount rate affects the Capital Recovery Factor (CRF) directly, while this parameter is in turn inversely related to NPC.

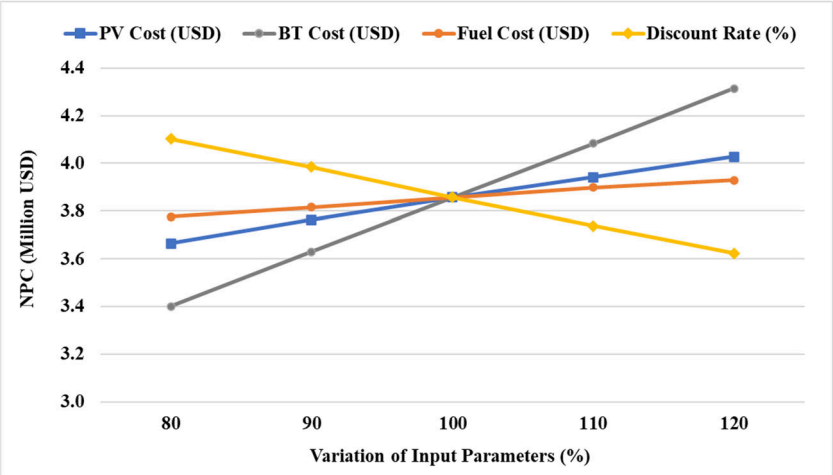

Figure 21. Impact on NPC due to variations in input parameters.

4.6.2. Impact on COE Due to Input Variables

According to Figure 22, the COE changes in the same direction as the variations in input parameters. The percentage change in COE is in line with that of the NPC for fuel, PV, and battery costs. However, the cost of energy and the net present cost behave differently; the former is directly proportional to the discount rate, and the percentage change in the COE is more than double that of the NPC, indicated by the steeper slope. This is because the discount rate directly influences the CRF, which is proportional to both the total annualized cost and the COE. A ±20% variation in fuel cost results in a negligible change in COE of approximately ±2–3%, while a ±20% variation in PV cost leads to a slightly higher change of approximately ±4–7%. However, a ±20% variation in battery cost causes a significant COE variation between ±8 and 20%. Similar trends within different ranges are reported elsewhere [17]. When the load is reduced by 20%, the variation in COE is relatively slight at around 6.7%. This suggests that although a larger HRES will be technically capable of meeting lower load demands more efficiently, COE will slightly increase due to factors such as investment and maintenance costs. However, when the load is increased by 20%, the COE increases by approximately 33%. This drastic increase is due to higher running and maintenance costs associated with greater reliance on the DG at elevated loads.

4.6.3. Impact on NPC and RF Due to Variations in Load

While maintaining a steady supply, the HRES can manage load fluctuations. The load of the proposed site is changed by ±20% to evaluate its effect on the NPC and RF. Changes in load demand have a small effect on NPC, as the system's reliance on batteries rather than DGs reduces the effect of fuel consumption variations. Figure 23 illustrates the impact of this load variation on net present cost and the renewable fraction. When the load decreases by 10% and 20%, the NPC decreases by almost the same percentage. However, when the load increases by 10% and 20%, the NPC rises at a rate nearly double that of the load increase, as evidenced by the steeper slope. The RF declines sharply as the load multiplier increases when demand exceeds the renewable energy capacity. As the load multiplier increases, the total electricity demand rises. Because the most cost-effective design consists of PV/DG/BT and PV generation is limited to daytime, the system increasingly relies on DG to meet additional demand, reducing the RF. Moreover, the PD method plans ahead for the next load and power generation, enabling it to operate at the lowest possible cost without sacrificing system reliability. When the load is gradually increased past that threshold, the available renewable energy will not be enough to supply the load, and therefore the system must rely more on DG as a way to stabilize the grid, i.e.,

Mode 2 of Figure 7. Consequently, RF experiences a steep decline as fossil fuel consumption increases. NPC ranges from 19% to 37% compared to the reference value because of the HRES's heavy reliance on batteries and the DG under the PD strategy to supply the load. For a 20% load reduction relative to the reference level, RF shows little variation. On the other hand, when the load is increased by 20%, the RF value decreases [93] because the power production of the PV is discontinuous and limited to only daylight hours. As such, extra demand must be satisfied mainly by the battery and the DG.

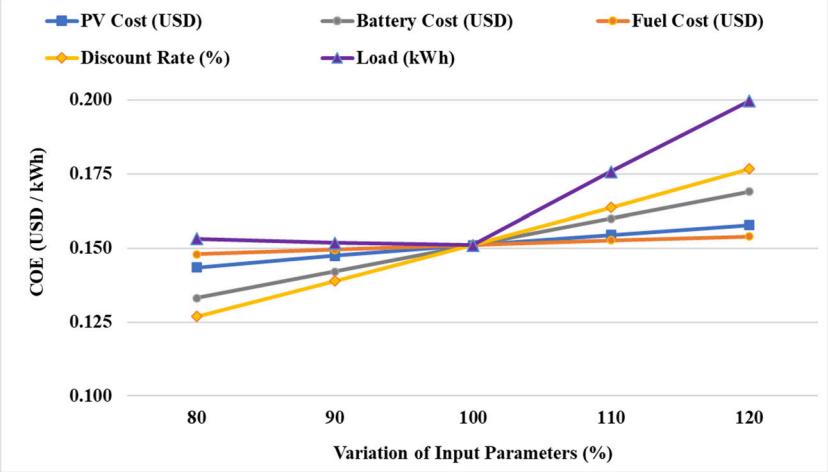

Figure 22. Impact on COE due to variations in input parameters.

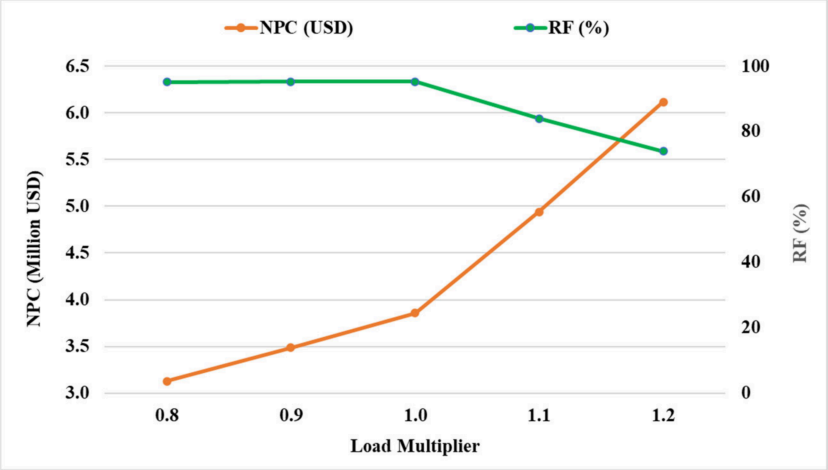

Figure 23. Effect of change in load demand on NPC and RF.

4.6.4. Impact on Lifetime Degradation and Cycle Performance Due to Ambient Temperature

A sensitivity analysis of ambient temperature (13 °C to 33 °C), with 22.67 °C as the reference temperature for Chinyunyu, is conducted to assess its effect on battery parameters (Table 11). The results show that temperature is one of the main factors affecting both PV performance and battery behavior. NPC and COE for all three battery types increase with rising temperature due to lower PV efficiency, leading to higher installed capacity requirements and faster battery degradation, including increased internal resistance and capacity loss from accelerated chemical aging at high temperatures. This results in rapid depletion of their energy throughputs. The impact is greatest for LA batteries, whose lifespan is reduced by 33%, requiring the most frequent replacement. LC occupies an intermediate position, with its lifespan shortened by 40%, yielding fewer replacements

than LA. In contrast, Li-ion batteries exhibit a nearly constant full lifespan of approximately 15 years, indicating greater thermal resilience. They have the lowest replacement frequency with the highest annual throughput given their larger lifetime throughput ceiling, as shown in Table 6. Lithium-ion batteries' longer lifecycle enables deeper discharge, and they are less sensitive to temperature changes. These results corroborate those of [94], indicating that lithium-ion batteries are well-suited to the Zambian high-temperature environment. Although Li-ion batteries offer the best economic performance, their deployment requires battery management systems, safe handling, diagnostic skills, local technician training, and clear maintenance contracts [10]. Because battery replacement is one of the dominant recurring cost streams aggregated into the NPC, the wide spread in replacement frequency across the three chemistries is one of the primary reasons they generate markedly different NPC and COE, as discussed in Sections 4.1–4.3.

Table 11. Impact on battery lifetime degradation due to ambient temperature.

445 W PV Panel with Lithium-Ion Battery					
Amb. Temp (°C)	13	18	22.67	28	33
PV (kW)	994	910	924	936	964
Battery (kWh)	437	439	439	439	438
NPC (USD million)	3.827336	3.840097	3.856895	3.874040	3.894192
COE (USD/kWh)	0.1499	0.1504	0.1510	0.1517	0.1525
RF (%)	96.0	95.2	95.2	95.1	95.1
Life (Years)	15	15	15	15	15
445 W PV Panel with Lead Carbon Battery					
PV (kW)	728	676	729	702	732
Battery (kWh)	470	496	482	490	486
NPC (USD million)	9.998493	10.011150	10.021900	10.034860	10.048100
COE (USD/kWh)	0.3916	0.3921	0.3925	0.3930	0.3935
RF (%)	43.5	43.5	43.5	43.5	43.5
Life (Years)	9.94	10.3	10.1	10.2	10.1
445 W PV Panel with Lead Acid Battery					
PV (kW)	676	651	633	649	694
Battery (kWh)	146	152	156	156	154
NPC (USD million)	10.093960	10.109660	10.118200	10.132330	10.147440
COE (USD/kWh)	0.3953	0.3959	0.3962	0.3968	0.3974
RF (%)	33	33.1	33.1	33.1	33.2
Life (Years)	2.97	2.98	3.00	3.00	2.99

4.6.5. Impact on NPC and COE Performance Due to Renewable Variability and Battery Life

Because the optimal HRES model is significantly influenced by solar PV and the battery used, uncertainty in renewable resource outputs and component lifetimes is analyzed in the sensitivity analysis. Solar radiation varied by 20% around the base value, ranging from 5.63 kWh/m^2/day to 4.52 kWh/m^2/day (−20%) and from 6.76 kWh/m^2/day to 8.10 kWh/m^2/day (+20%), representing the typical climatic variability experienced in Zambia [49]. Similarly, the battery and converter lifetimes varied from 15 years to 12 years (20%) and 18 years (20%). This is within the typical operating period of batteries in Sub-Saharan mini-grids [94].

From Figure 24, it is inferred that a 20% drop in solar radiation substantially raises system expenses, with increases of 5.4% and 5.2% in NPC and COE. Conversely, a 20% increase in radiation level decreases NPC and COE by approximately 3.9%. This contrast indicates that the HRES is sensitive to climate variability. However, when examining the effect of battery life duration, the NPC and COE increase by about 13. 8% when duration is reduced by 20% and decrease up to 9.9% with increasing duration. Therefore,

HRES economics are more significantly affected by battery degradation, requiring effective periodic system performance monitoring procedures.

4.6.6. Ranking of Parameters Influencing NPC and COE

Table 12 ranks the sensitivity of NPC and COE to the ±20% variation for the seven parameters investigated. Load demand is the most influential factor, with a +20% increase in load more than tripling both the NPC and COE. This is because the PD strategy is configured to meet load demand through the battery bank, which must supply the additional load rather than the diesel generator. Battery cost and battery life rank second, forming a near-overlapping band and dominating the cost bundle. Their values exceed the effect of the discount rate on NPC but are comparable to its effect on COE. Solar radiation and PV cost rank in the middle due to the irregular nature of solar power. Fuel cost appears at the bottom of the rankings, confirming the earlier observation that under the PD strategy the diesel generator accounts for only a small share of the lifetime fuel throughput. These findings suggest that future cost reductions in battery technologies and improvements in their lifespan would provide the greatest economic benefits for HRESs.

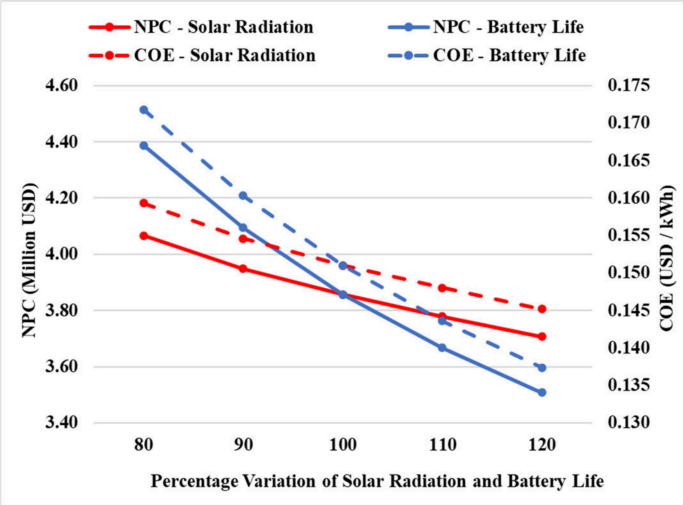

Figure 24. Effect of renewable variability and battery life on NPC and COE.

Table 12. Ranked parameters influencing NPC and COE.

Rank	Parameter	NPC Variation Range (%)	COE Variation Range (%)	Relationship
1	Load Demand	19–37	6.7–33	Direct Asymmetric
2	Battery Cost	5–12	8–20	Direct
3	Battery Lifetime	9.9–13.8	9.9–13.8	Direct Asymmetric
4	Discount Rate	6.5	>13%	NPC-Inverse COE-Direct
5	Solar Radiation	3.9–5.4	3.9–5.2	Direct Asymmetric
6	PV Cost	2–5	4–7	Direct
7	Fuel Cost	1–2	2–3	Direct

4.6.7. Impact on NPC and COE Performance Due to Capacity Shortage

Dependability of the proposed HRES was investigated under different capacity shortage levels (0%, 3%, and 5%) across three system configurations. To ensure that critical loads, such as health centers and schools, always have power, zero-capacity shortage was

selected as an option [95]. However, a 2–5% shortage is generally permissible for rural household electrification to reduce system costs [96]. As the considered area includes both essential services and residential loads, all configurations were tested at these three reliability levels, the results of which are presented in Table 13. For the PV/WT/DG/BT and PV/DG/BT HRESs, component sizes did not vary across different capacity shortage levels because the diesel generator could cover peak demand. On the other hand, the PV/BT system experienced large drops in both PV and battery capacities as the allowed shortage was increased. More specifically, PV capacity fell from 2484 kW to 1105 kW (55%) and then to 998 kW 9 (a further 9.7%), while battery units were reduced from 534 to 434 (18.7%) and then to 416 (a further 4.1%). Likewise, NPC fell from USD 5.27 million to USD 3.47 million (34%) and then to USD 3.27 million (a further 5.9%), while COE dropped from USD 0.2065/kWh to USD 0.1397/kWh (32.3%) and finally to USD 0.1330/kWh (a further 4.3%).

Table 13. Assessment of system reliability using capacity shortages of 0%, 3%, and 5%.

	Configuration								
	PV/WT/DG/BT			**PV/DG/BT**			**PV/BT**		
	Capacity Shortage			**Capacity Shortage**			**Capacity Shortage**		
Item	**0%**	**3%**	**5%**	**0%**	**3%**	**5%**	**0%**	**3%**	**5%**
Solar PV Panels (kW)	938	938	938	924	924	924	2484	1105	998
Wind Turbine (kW)	2	2	2	Nil	Nil	Nil	Nil	Nil	Nil
Diesel Generator (kW)	350	350	350	350	350	350	Nil	Nil	Nil
Li-ion Battery (Nos.)	444	444	444	439	439	439	534	436	416
Converter (kW)	344	344	344	344	344	344	344	344	344
NPC (USD million)	3.899516	3.899516	3.899516	3.856895	3.856895	3.856895	5.267647	3.474054	3.269866
COE (USD/kWh)	0.1527	0.1527	0.1527	0.1510	0.1510	0.1510	0.2065	0.1397	0.1330
Capacity Shortage (%)	0	0	0	0	0	0	0.1	3.07	5.71
Unmet Load (%)	0	0	0	0	0	0	0.08	2.58	3.74
Excess Electricity (%)	44.1	44.1	44.1	43.3	43.3	43.3	78.4	52.6	48.2
Renewable Fraction (%)	95.5	95.5	95.5	95.2	95.2	95.2	100	100	100

Higher-level capacity shortages can improve economic performance. However, they cause major reliability problems. For example, at capacity shortages of 3% and 5%, the system shows power outages of approximately 263 h (11 days) and 438 h (19 days) per year. The PV/BT system relies on a single intermittent energy source, and therefore reliability sacrifices are unacceptable for critical applications. Thus, after weighing both economic and reliability factors, the 924 kW-PV/350 kW-DG/439 Li-ion-BT/344 kW converter system operating under the PD strategy with no capacity shortage is considered the most suitable solution.

4.7. Social Benefits

The optimized PV/DG/BT configuration can offer benefits beyond cost and emissions reductions. Reliable electricity can improve clinical operations through vaccine and medicine refrigeration, emergency lighting, phone charging, and radio communication [51]. The school can benefit from improved lighting and computer use, leading to longer study hours, while households can benefit from safer lighting and reduced reliance on candles and kerosene, improving indoor air quality. Productive uses such as milling, water pump-

ing, refrigeration, and small appliances can also create local income opportunities [84]. While electricity may not immediately replace charcoal and firewood for cooking, reliable access can reduce reliance on candles, dry-cell batteries, kerosene lamps, and small fossil fuel generators [9]. These indirect benefits can contribute to improved local air quality and reduced fire risk, as well as improved welfare, service delivery, and rural economic resilience.

4.8. Policy Recommendations

On a policy and planning level, the results of this study suggest that Zambia's rural electrification strategy, delivered through its Rural Electrification Master Plan (REMP 2025–2030) [97] and large-scale electricity access through grid extension and off-grid options, should continue working toward the deployment of hybrid mini-grids to accelerate universal access. To help address high upfront investment requirements, policy measures such as targeted subsidies, risk-sharing mechanisms, and innovative financing can be adopted to attract private investment. On an engineering level, to ensure cost-effective, reliable, and sustainable hybrid mini-grids, the selection of high-power PV modules, long-life battery technologies, and predictive dispatch strategies should be prioritized.

Beyond the battery-anchored architectures evaluated here, regional analyses increasingly view green hydrogen as a complementary vector for decarbonization and long-duration storage in evolving energy mixes. Recent studies highlight the broader investment case for green hydrogen in Sub-Saharan Africa (SSA) [98], its role in extending hybrid mini-grids for remote energy access [39,99], and SSA's current readiness in terms of planning, funding, and partnerships [80,100]. Alongside previously mentioned subsidies, risk sharing, and innovative financing instruments, this study provides a quantitative baseline for Zambia's REMP 2025–2030 policy framework. The techno-economic metrics used in our study therefore serve as a quantitative baseline for future planning cycles to evaluate the incremental benefits of coupling long-duration hydrogen storage with this lowest-cost hybrid architecture.

5. Conclusions

An extensive techno-economic and environmental assessment of the proposed HRES was conducted by evaluating various PV panel ratings, battery types, dispatch strategies and system configurations. The findings demonstrate that sustainable rural electrification requires an integrated approach that considers reliability, cost, emissions, technology lifetime, affordability, and practical applicability. Using the DG as a backup in HRES significantly lowers emissions and reduces system costs. The 445 W PV panel offers the lowest NPC and COE, whereas Li-ion batteries outperform LA and LC batteries in economic performance, especially under the PD scenario. In summary, the PV/DG/BT system (Case-2) with a 445 W PV panel and a Li-ion battery under the PD strategy yields the most cost-effective solution, with an NPC of USD 3.857 million and a COE of USD 0.151/kWh compared to the DG-only system. These findings suggest that rural electrification initiatives could benefit from increased emphasis on hybrid mini-grid deployment. Policy measures such as targeted subsidies, fiscal incentives, and financing mechanisms could facilitate wider deployment. Furthermore, incorporating lifecycle environmental considerations into planning could enhance alignment with national climate and sustainability objectives.

The outputs from this study are site-specific and depend on the climate conditions, renewable energy resources, load profile, component costs and techno-economic assumptions relevant to Chinyunyu in Zambia. Because of this, the optimal system configuration of a 445 W PV module, Li-ion battery technology and the predictive dispatch strategy obtained in this study is specific to the study site. For other locations with different renewable re-

source availabilities, load profiles, component costs and relevant market circumstances will reveal different optimal configurations of the hybrid system. While the benefits of larger capacity PV modules, lithium-ion batteries and predictive dispatch strategy are expected to be universally relevant under similar circumstances, their relative performance characteristics may change according to factors such as fuel prices, types of batteries, market conditions, policy constraints and others. Given that the study site is currently unelectrified and that grid extension is not economically feasible due to dispersed demand and low return on investment, the hybrid renewable energy system proposed in this study seems to be an economical decentralized source of electricity. However, the implementation of such a technology depends on favorable policies, financing avenues and institutional capacity development which should also be considered in other similar projects.

Future research should extend the proposed framework by incorporating stochastic renewable resource models and field-based electricity demand data to better capture weather variability and demand uncertainty. Validation of other subsystem components against a second simulator would enable comprehensive validation of the complete HRES. More detailed physics-based battery degradation models that encompass critical battery parameters and apply multi-objective optimization would also allow for consideration of economic, technical, environmental, and social objectives. These enhancements would improve the robustness and broader applicability of the proposed framework for hybrid mini-grid planning.

Author Contributions: Conceptualization, F.D.Y. and M.M.; Methodology, S.S.V. and M.R.; Software, S.S.V.; Formal analysis, I.N.S. and M.K.; Resources, N.C.S.; Data curation, N.C.S.; Writing—original draft, S.S.V.; Writing—review & editing, M.M., I.N.S., M.R. and M.K.; Supervision, F.D.Y., M.M., I.N.S. and M.R. All authors have read and agreed to the published version of the manuscript.

Funding: This research received no external funding.

Institutional Review Board Statement: Not applicable.

Informed Consent Statement: Not applicable.

Data Availability Statement: The data presented in this study are available on request from the corresponding author. The data are not publicly available due to privacy or ethical restrictions.

Conflicts of Interest: The authors declare no conflict of interest.

Nomenclature

A	constant scaled such that the degradation varies from zero to the specified capacity
B	constant scaled such that the degradation varies from zero to the specified capacity degradation limit over the course of the lifetime (set by the manufacturer)
c	Storage capacity ratio of the battery
$C_{ann.tot}$	Total yearly cost of the HRES ($/y)
C_{NPC}	Net Present Cost ($)
CRF	Capital Recovery Factor (%)
d	Activation energy constant (sensitivity of battery chemistry to heat)
DoD	Depth of discharge (ranging 0–1)
E_{Demand}	Load demand (kWh)
$E_{embodied}$	Emissions arising from the manufacturing and replacement of system components (PV modules, batteries, etc.) (kg-CO_2)
$E_{operation}$	Emissions from system operation, primarily diesel fuel consumption as obtained from HOMER simulations. (kg-CO_2)

E_{served}	Total electrical energy supplied in a year (kWh/y)
$E_{transport}$	Emissions from transportation of system components to the project site (kg-CO_2)
F	Generator fuel consumption (Units)
$F_{0,DG}$	Coefficient of fuel curve intercept (units/h/kW)
$F_{1,DG}$	Gradient of the fuel curve (units/h/kW)
f_{PV}	Derating factor accounting for losses attributed to wire losses, shadow, dust, temperature, etc. (%)
G_S	Incident radiation at 1 (kW/m^2)
G_T	Hourly incident radiation received by the solar PV array under working conditions (kW/m^2)
$G_{T,NOCT}$	Solar radiation at 0.8 (kW/m^2)
H	Wind turbine Hub height (m)
$H_{0,avg}$	At the top of the Earth'satmosphere, radiation on a horizontal plane (kWh/m^2/day)
H_{avg}	Average radiation on the Earth's horizontal surface (kWh/m^2/day)
i	Real discount rate (%)
I_{max}	Battery's peak charging current (A)
k	Storage rate Constant (h^{-1})
k_t	Rate of increase in the time and temperature degradation variable
K_t	Clearness index (ranges between 0 and 1)
N	Year Number
N_C	Number of battery discharge cycles
N_{Batt}	Number of batteries
$n_{Load\text{-}i,j}$	The number of the ith load under the jth type
NPC	Net Present Cost (USD $)
$P_{Batt,Cmax,kbm}$	The maximum charge rate (kW) corresponds to the storage charge power.
$P_{Batt,Cmax,mcr}$	The storage charge power (kW) that corresponds to the highest charge current
P_{DG}	Generator electrical power output (kW)
P_{in}	Power input (kW)
P_o	Power output (kW)
P_{PV}	Power output from PV Array (kW)
P_r	Rated power of the wind turbine (kW)
P_W	Actual power generated by the wind turbine (kW)
$P_{WT,STP}$	Turbine power output at standard conditions (kW)
P_{WTG}	Wind turbine power output (kW)
Q	SoC at the end of the time interval (kWh)
Q1	SoC at the beginning of the time interval and above SoC_{min} (kWh)
R_{Proj}	Project lifetime (Years)
R_{Proj}	Project life time (Years)
$r_{rating\text{-}i,j}$	The rating of ith load under j^{th} type (kW)
T	Temperature
T_a	Ambient temperature (°C)
$T_{a,NOCT}$	Ambient temperature at 20 °C
T_C	PV module cell temperature under the current time step (°C)
$T_{C,NOCT}$	NOCT (°C)
$T_{C,STC}$	Temperature of the PV array at 25 °C
$T_{Duration\text{-}i,j}$	The duration of ith load under j^{th} type (h)
U_L	Heat transfer coefficient to surroundings (kW/m^2 °C)
V	Wind speed at the desired height (m/s)
V_{Base}	Wind speed at a base height, H_{Base} (m/s)
$V_{Cut\text{-}in}$	Cut-in speed (m/s)
$V_{Cut\text{-}out}$	Furlong (or cut-out) speed (m/s)

V_{nom}	Nominal voltage of the battery (V)
Vr	Rated wind speed (m/s)
Y_{DG}	Generator rated capacity (kW)
Y_{DG}	Rated power of the DG (kW)
Y_{PV}	Rating of PV array under STC (kW)
Greek	
Δt	Time step duration (h)
α	Absorptance of the PV modules (%)
α_c	Battery peak charging rate (A/Ah)
α_p	PV array's temperature coefficient of power (%/°C)
α_w	Power law exponent or power law coefficient, which accounts for wind speed with height above the ground, and typically ranges between 0.1 and 0.4.
$\eta_{Batt,c}$	Efficiency of charge storage in battery (%)
η_{in}	Efficiency of converter (%)
ρ	Actual air density (kg/m^3)
ρ_0	Air density at standard conditions (1.225 kg/m^3)
τ	Solar transmittance of the PV modules (%)
Abbreviations	
avg	Average
batt	Battery
BT	Battery
kbm	Kinetic Battery Model
max	Maximum
mcc	Peak Charge Current (A)
mcr	Peak Charge Rate (A/hr)
proj	Project

Appendix A

Table A1. Optimized results of LA, LC and Li-ion batteries based HRES with 445 W panel under the LF, CC, CD and PD strategies.

Dispatch Strategy—Load Following									
Battery Type	**Lead Acid**			**Lead Carbon**			**Li-Ion**		
Case No	1	2	3	1	2	3	1	2	3
PV (kW)	549	552	3055	544	504	1092	1076	1017	2478
Wind (Nos)	3			1	-	-	1	-	
DG (kW)	350	350		350	350	-	350	350	
Battery (Nos.)	180	178	2766	138	136	2450	447	439	534
Converter (kW)	344	344	344	344	344	344	344	344	344
Dispatch Strategy—Cycle Charging									
Battery Type	**Lead Acid**			**Lead Carbon**			**Li-ion**		
Case No	1	2	3	1	2	3	1	2	3
PV (kW)	560	547	3055	699	585	1092	1329	1326	2478
Wind (Nos)	2	-	-	3	-	-	1	-	-
DG (kW)	350	350	-	350	350	350	350	350	-
Battery (Nos.)	156	164	2766	120	124	2450	439	445	534
Converter (kW)	344	344	344	344	344	344	344	344	344

Table A1. *Cont.*

Dispatch Strategy—Combined Dispatch									
Battery Type	**Lead Acid**			**Lead Carbon**			**Li-ion**		
Case No	1	2	3 *	1	2	3 *	1	2	3 *
PV (kW)	634	627	-	768	703	-	1188	1193	-
Wind (Nos)	2	-	-	1	-	-	1	-	-
DG (kW)	350	350	-	350	350	-	350	350	-
Battery (Nos.)	44	40	-	22	22	-	432	431	-
Converter (kW)	344	344	-	344	344	-	344	344	-
Dispatch Strategy—Predictive Dispatch									
Battery Type	**Battery Type**			**Battery Type**			**Battery Type**		
Case No	1	2	3	1	2	3	1	2	3
PV (kW)	780	633	3105	700	729	1092	938	924	2484
Wind (Nos)	1	-	-	1	-	-	2	-	-
DG (kW)	350	350	-	350	350	-	350	350	-
Battery (Nos.)	150	156	2760	494	482	2450	444	439	534
Converter (kW)	344	344	344	344	344	344	344	344	344

* The CD Strategy does not yield any results for Case 3 as it requires at least one generator within the configuration, hence appears blank in the table.

Table A2. Comparison of the LA, LC and Li-ion battery performance under the PD strategy.

Battery Type	**Lead–Acid**			**Lead–Carbon**			**Li-Ion**		
Parameter	**Case-1**	**Case-2**	**Case-3**	**Case-1**	**Case-2**	**Case-3**	**Case-1**	**Case-2**	**Case-3**
Nominal Capacity (kWh)	180	187	3312	1298	1266	6435	2309	2283	2777
Nominal Capacity (Nos.)	150	156	2760	494	482	2450	444	439	534
Usable Nominal Capacity (kWh)	144	150	2650	1038	1013	5148	2078	2055	2499
Lifetime Throughput (kWh)	181,800	189,072	3,345,120	1,128,839	1,101,418	5,598,495	9,267,268	9,292,427	9,452,132
Expected Life (y)	2.99	3	4.93	10.3	10.1	8.15	15	15	15
Energy in (kWh/y)	65,921	68,444	735,092	118,565	117,904	743,040	620,925	622,544	632,303
Energy out (kWh/y)	56,036	58,120	625,974	100,787	100,225	633,186	614,721	616,324	626,983
Losses (kWh/y)	9708	10,080	107,049	16,488	16,420	105,157	3900	3943	3551
Annual Throughput (kWh/y)	60,779	63,105	678,964	109,319	108,710	686,786	617,818	619,428	630,142

Table A3. Operational CO_2 and pollutant emissions of the DG-only and optimal feasible HRES under different strategies.

		Dispatch Strategies							
	Base Case	**LF**		**CC**		**CD**		**PD**	
Emissions (kg/y)	**DG Only**	**Case-1**	**Case-2**	**Case-1**	**Case-2**	**Case-1**	**Case-2**	**Case-1**	**Case-2**
CO_2	793,467	19,843	23,882	27,119	24,620	27,195	27,389	28,225	30,291
CO	5002	125	151	171	155	171	173	178	191

Table A3. *Cont.*

	Dispatch Strategies								
	Base Case	**LF**		**CC**		**CD**		**PD**	
Emissions (kg/y)	**DG Only**	**Case-1**	**Case-2**	**Case-1**	**Case-2**	**Case-1**	**Case-2**	**Case-1**	**Case-2**
UHC	218	5.46	6.57	7.46	6.77	7.48	7.53	7.76	8.33
PM	30.3	0.758	0.912	1.04	0.941	1.04	1.05	1.08	1.16
SO_2	1943	48.6	58.5	66.4	60.3	66.6	67.1	69.1	74.2
NOx	4698	117	141	161	146	161	162	167	179

References

1. Rinkesh, K. Causes, Effects and Solutions of Depletion of Natural Resources. Conserve Energy Future. 2020. Available online: https://www.conserve-energy-future.com/causes-effects-solutions-depletion-natural-resources.php (accessed on 11 May 2026).
2. Samy, M.M.; Elkhouly, H.I.; Barakat, S. Multi-objective optimization of hybrid renewable energy system based on biomass and fuel cells. *Int. J. Energy Res.* **2020**, *44*, 2463–2476. [CrossRef]
3. Hasan, S.; Meem, A.I.; Islam, M.S.; Proma, S.S.; Mitra, S.K. Comparative techno-economic analyses and optimization of standalone and grid-tied renewable energy systems for South Asia and Sub-Saharan Africa. *Results Eng.* **2024**, *21*, 101964. [CrossRef]
4. Tazay, A.F.; Samy, M.M.; Barakat, S. A techno-economic feasibility analysis of an autonomous hybrid renewable energy sources for university building at Saudi Arabia. *J. Electr. Eng. Technol.* **2020**, *15*, 2151–2160. [CrossRef]
5. Fofang, T.F.; Tanyi, E. Design and simulation of off-grid solar/mini hydro renewable energy system using HOMER Pro software: Case for Muyuka rural community. *Int. J. Eng. Res. Technol.* **2020**, *9*, 1–6.
6. Ali, M.F.; Sheikh, M.R.I.; Akter, R.; Islam, K.M.N.; Ferdous, A.H.M.I. Grid-connected hybrid microgrids with PV/wind/battery: Sustainable energy solutions for rural education in Bangladesh. *Results Eng.* **2025**, *25*, 103774. [CrossRef]
7. Kapole, F.; Mudenda, S.; Jain, P. Study of Major Solar Energy Mini Grid Initiatives in Zambia. *Results Eng.* **2023**, *18*, 101095. [CrossRef]
8. United Nations. The Sustainable Development Goals (SDG) Report 2023. Available online: https://unstats.un.org/sdgs/report/2023/The-Sustainable-Development-Goals-Report-2023.pdf (accessed on 1 September 2023).
9. Yakubu, S.; Samikannu, R.; Yahya, A.; Badruddin, I.A.; Kamangar, S.; Kadarmydeen, M.B.; Kwarteng, M.; Ladu, N.S.D.; Wetajega, S.D. Feasibility design, comparative evaluation, and energy consumption prediction of standalone hybrid energy system for rural electrification in Ghana using machine learning models. *Results Eng.* **2025**, *25*, 104269. [CrossRef]
10. Ministry of Energy. *National Energy Policy*; Ministry of Energy, Government Republic of Zambia: Lusaka, Zambia, 2019.
11. World Bank. Tracking SDG 7: The Energy Progress Report—Access to Electricity (% Population—Zambia); Washington, DC, World Bank Open Data, 2023. Available online: https://data.worldbank.org/indicator/EG.ELC.ACCS.ZS?locations=ZM (accessed on 5 September 2023).
12. Mwansa, K.; Gheewala, S.H. Techno-economic assessment of bioenergy options using crop and forest residues for non-electrified rural growth centers in Zambia. *Biomass Bioenergy* **2021**, *145*, 105944. [CrossRef]
13. Virdy, S.S.; Yamba, F.D. An investigation into barriers affecting the implementation of the clean development mechanism (CDM) in Zambian firms. *Zamb. Eng.* **2013**, *46*, 20–32.
14. Ministry of Education. *Scaling up Renewable Energy in Low-Income Countries—Investment Plan—Climate Investment Plan*; Republic of Zambia, Ministry of Energy: Lusaka, Zambia, 2019.
15. Barakat, S.; Emamb, A.; Samy, M.M. Investigating grid-connected green power systems' energy storage solutions in the event of frequent blackouts. *Energy Rep.* **2022**, *8*, 5177–5191. [CrossRef]
16. Pujari, H.K.; Chinna Alluraiah, N.; Pasala, G.; Bajaj, M.; Kumar, P.S.; Ch, N.S.K.; Blazek, V. Techno-economic optimization and sensitivity analysis of off-grid hybrid renewable energy systems: A case study for sustainable energy solutions in rural India. *Results Eng.* **2025**, *25*, 103674. [CrossRef]
17. Dhavala, R.K.; Suresh, H.N.; Rajanna, S.; Ramesh, M. Effects of different batteries and dispatch strategies on performance of standalone systems. *Energy Storage* **2021**, *4*, e306. [CrossRef]
18. Eteiba, M.B.; Barakat, S.; Samy, M.M.; Wahba, W.I. Optimization of an off-grid PV/biomass hybrid system with different battery technologies. *Sustain. Cities Soc.* **2018**, *40*, 713–727. [CrossRef]
19. Dibaba, H.D. Business Model for Microgrids in Sub-Saharan Africa Rural Areas: A Case Study in Revon C, Namibia. Master's Thesis, LUT University, Lappeenranta, Finland, 2019. Available online: https://lutpub.lut.fi/handle/10024/160125 (accessed on 29 April 2026).

20. Kumar, P.P.; Saini, R.P. Optimization of an off-grid integrated hybrid renewable energy system with different battery technologies for rural electrification in India. *J. Energy Storage* **2020**, *32*, 101912. [CrossRef]
21. Gebrehiwot, K.; Mondal, M.A.H.; Ringler, C.; Gebremeskel, A.G. Optimization and cost-benefit assessment of hybrid power systems for off-grid rural electrification in Ethiopia. *Energy* **2019**, *177*, 234–246. [CrossRef]
22. Manjunath, H.N.S.; Rajanna, S. Reduction of mislead power and mismatch power loss under partial shading conditions using novel square matrix shade dispersion technique. *Sol. Energy* **2020**, *207*, 1364–1383. [CrossRef]
23. Samy, M.M.; Elazazy, M.; Nabil, M. Optimal sizing and techno-economic analysis of reverse osmosis desalination systems based on PV/wind green energy system. *J. Eng. Sci. Sustain. Ind. Technol.* **2024**, *2*, 33–39. [CrossRef]
24. Khan, F.A.; Pal, N.; Saeed, S.H.; Yadav, A. Modelling and Techno-Economic Analysis of Standalone SPV/Wind Hybrid Renewable Energy System with Lead-Acid Battery Technology for Rural Applications. *J. Energy Storage* **2022**, *55*, 105742. [CrossRef]
25. Alshammari, N.; Samy, M.M.; Asumadu, J. Optimal economic analysis study for renewable energy systems to electrify remote regions in the Kingdom of Saudi Arabia. In *Proceedings of the Twentieth International Middle East Power Systems Conference (MEPCON)*; IEEE: Piscataway, NJ, USA, 2018.
26. Arabali, A.; Gofrani, M.; Etezadi Amoli, M.; Fadali, M.S. Stochastic performance assessment and sizing of a hybrid power system of solar/wind energy/storage. *IEEE Trans. Sustain. Energy* **2014**, *5*, 363–371. [CrossRef]
27. Guven, A.F.; Abdelaziz, A.Y.; Samy, M.M.; Barakat, S. Optimizing energy dynamics: A comprehensive analysis of hybrid energy storage systems integrating battery banks and supercapacitors. *Energy Convers. Manag.* **2024**, *312*, 118560. [CrossRef]
28. Redouane, A.; Saou, R.; Belkhier, Y.; Oukaour, A. Integration of a novel Vernier-DSPM generator in a grid-connected hybrid renewable energy system with battery storage. *Results Eng.* **2025**, *25*, 103814. [CrossRef]
29. Bukar, A.I.; Tan, C.W.; Lau, K.Y. Optimal sizing of an autonomous photovoltaic/wind/battery/diesel generator microgrid using grasshopper optimization algorithm. *Sol. Energy* **2019**, *188*, 685–696. [CrossRef]
30. Barakat, S.; Osman, A.I.; Tag-Eldin, E.; Telba, A.A.; Abdel Mageed, H.M.; Samy, M.M. Achieving green mobility: Multi-objective optimization for sustainable electric vehicle charging. *Energy Strategy Rev.* **2024**, *53*, 101351. [CrossRef]
31. Guven, A.F.; Yorukeren, N.; Samy, M.M. Design optimization of a stand-alone green energy system of university campus based on Jaya-Harmony Search and Ant Colony Optimization algorithms approaches. *Energy* **2022**, *253*, 124089. [CrossRef]
32. Vendoti, S.; Muralidhar, M.; Kiranmayi, R. Techno-economic analysis of off-grid solar/wind/biogas/biomass/fuel cell/battery system for electrification in a cluster of villages by HOMER software. *Environ. Dev. Sustain.* **2020**, *23*, 351–372. [CrossRef]
33. Sinha, S.; Chandel, S.S. Review of recent trends in optimization techniques for solar photovoltaic-wind based hybrid energy systems. *Renew. Sustain. Energy Rev.* **2015**, *50*, 755–769. [CrossRef]
34. Iqbal, M.; Azam, M.; Naeem, M.; Khwaja, A.S.; Anpalagan, A. Optimization classification, algorithms and tools for renewable energy: A review. *Renew. Sustain. Energy Rev.* **2014**, *39*, 640–654. [CrossRef]
35. Silinto, B.F.; Yamu, C.; Zuidema, C.; Faaij, A.P.C. Hybrid renewable energy systems for rural electrification in developing countries: A review on energy system models and spatial explicit modelling tools. *Renew. Sustain. Energy Rev.* **2025**, *207*, 114916. [CrossRef]
36. Abdulkarim, A.; Abdelkader, S.M.; Morrow, D.J.; Amuda, S.A.Y.; Madugu, I.S.; Falade, A.J.; Saminu, S.; Adediran, Y.A. Effects of PV and Battery Storage Technologies on the Optimal Sizing of Renewable Energy Microgrid. *Elektr. J. Electr. Eng.* **2018**, *17*, 1–8. [CrossRef]
37. Barakat, S.; Samy, M.M.; Eteiba, M.B.; Whaba, W.I. *Viability Study of Grid-Connected PV/Wind/Biomass Hybrid Energy System for a Small Village in Egypt*; IEEE: Piscataway, NJ, USA, 2016. [CrossRef]
38. Patel, A.M.; Singal, S.K. Optimal component selection of integrated renewable energy system for power generation in stand-alone applications. *Energy* **2019**, *175*, 481–504. [CrossRef]
39. Wang, S.; Zhang, S.; Wen, S.; Fernandez, C. An Accurate State-of-Charge Estimation of Lithium-Ion Batteries Based on Improved Particle Swarm Optimization-Adaptive Square Root Cubature Kalman Filter. *J. Power Sources* **2024**, *624*, 235594. [CrossRef]
40. Katti, P.K.; Khedkar, M.K. Alternative Energy Facilities Based on Site Matching and Generation Unit Sizing for Remote Area Power Supply. *Renew. Energy* **2007**, *32*, 1346–1362. [CrossRef]
41. Chauhan, A.; Saini, R.P. Techno-Economic Feasibility Study on Integrated Renewable Energy System for an Isolated Community of India. *Renew. Sustain. Energy Rev.* **2016**, *59*, 388–405. [CrossRef]
42. Biramo, I. Energy-Water-Agriculture Nexus Mini Grids to Power Rural Productive Hubs in Sub-Saharan Africa—A Case Study of Walta Jalala Village in Bedeno Woreda of Ethiopia. Master's Thesis, European Solar Engineering School, Dalarna University, Falun, Sweden, 2020.
43. Khan, F.A.; Pal, N.; Saeed, S.H.; Yadav, A. Techno-economic and feasibility assessment of standalone solar photovoltaic/wind hybrid energy system for various storage techniques and different rural locations in India. *Energy Convers. Manag.* **2022**, *270*, 116217. [CrossRef]
44. Samy, M.M.; Emam, A.; Tag-Eldin, E.; Barakat, S. Exploring Energy Storage Methods for Grid-Connected Clean Power Plants in Case of Repetitive Power Outages. *J. Energy Storage* **2022**, *54*, 105307. [CrossRef]

45. Bhatt, A.; Ongsakul, W.; Madhu, N.M. Optimal Techno-Economic Feasibility Study of Net-Zero Carbon Emission Microgrid Integrating Second-Life Battery Energy Storage System. *Energy Convers. Manag.* **2022**, *266*, 115825. [CrossRef]
46. Mala, R.; Saini, R.P. Dispatch Strategies-Based Performance Analysis of a Hybrid Renewable Energy System for a Remote Area in India. *J. Clean. Prod.* **2020**, *259*, 120697. [CrossRef]
47. Chaurasia, R.; Gairola, S.; Pal, Y. Technical, Economic, and Environmental Performance Comparison Analysis of a Hybrid Renewable Energy System Based on Power Dispatch Strategies. *Sustain. Energy Technol. Assess.* **2022**, *53*, 102787. [CrossRef]
48. Rumbayan, M.; Kindangen, J.; Sambul, A.; Sompie, S.; Cross, J. Solar energy implementation in rural communities and its contributions to SDGs: A systematic literature review. *Unconv. Resour.* **2025**, *6*, 100180. [CrossRef]
49. NASA Prediction of Worldwide Energy Resources (POWER). 2026. Available online: https://power.larc.nasa.gov/ (accessed on 19 April 2026).
50. Zhao, B.; Wang, Y.; Luan, W.; Cai, H. Empowering data-driven PV system modeling and forecasting: A review of public benchmark datasets. *Glob. Energy Interconnect.* **2026**, *9*, 219–242. [CrossRef]
51. Quansah, A.D.; Dogbey, F.; Asilevi, P.J.; Baokye, P.; Darkwa, L.; Kwarteng, S.O.; Neuvam, Y.A.S.; Mensah, P. Assessment of solar radiation resource from the NASA-POWER reanalysis products for tropical climates in Ghana towards clean energy application. *Sci. Rep.* **2022**, *12*, 10684. [CrossRef] [PubMed]
52. Samy, M.M.; Barakat, S. *Hybrid Invasive Weed Optimization—Particle Swarm Optimization Algorithm for Biomass/PV Micro-Grid Power System*; IEEE: Piscataway, NJ, USA, 2019; ISBN 978-1-7281-5289-9.
53. Prinsloo, G. Scoping exercise to determine load profile archetype reference shapes for solar co-generation models in isolated off-grid rural African villages. *J. Energy South. Afr.* **2016**, *27*, 11–27. [CrossRef]
54. Stritzke, S.; Jain, P. The Sustainability of Decentralised Renewable Energy Projects in Developing Countries: Learning Lessons from Zambia. *Energies* **2021**, *14*, 3757. [CrossRef]
55. Akhtari, M.R.; Baneshi, M. Techno-Economic Assessment and Optimization of a Hybrid Renewable Co-Supply of Electricity, Heat, and Hydrogen System to Enhance Performance by Recovering Excess Electricity for a Large Energy Consumer. *Energy Convers.* **2019**, *188*, 131–141. [CrossRef]
56. HOMER Pro 3.14 User Manual. 2020. Available online: https://support.ul-renewables.com/homer-manuals-pro/index.html (accessed on 30 March 2024).
57. Das, B.K.; Hoque, N.; Mandal, S.; Pal, T.K.; Raihan, M.A. A Techno-Economic Feasibility of a Stand-Alone Hybrid Power Generation for Remote Area Application in Bangladesh. *Energy* **2017**, *134*, 775–788. [CrossRef]
58. Singh, S.; Singh, M.; Kaushik, S.C. Feasibility Study of an Islanded Microgrid in Rural Area Consisting of PV, Wind, Biomass, and Battery Energy Storage System. *Energy Convers. Manag.* **2016**, *128*, 178–190. [CrossRef]
59. Razmjoo, A.; Sumper, A.; Davarpanah, A. Energy Sustainability Analysis Based on SDGs for Developing Countries. *Energy Sources Part A Recovery Util. Environ. Eff.* **2019**, *42*, 1041–1056. [CrossRef]
60. Alayande, A.S.; Ignatius, O.; Omogoye, S.O. Homer Pro-Based Approach for Designing and Optimizing a Grid-Tied Hybrid Renewable Energy System for a Rural Community. *Arid Zone J. Eng. Technol. Environ.* 2025. Available online: https://www.researchgate.net/publication/389642373 (accessed on 29 April 2026).
61. Baneshi, M.; Hadianfard, F. Technoeconomic Feasibility Study of Hybrid Diesel/PV/Wind/Battery Electricity Generation Systems for Non-Residential Large Electricity Consumers under Southern Iran Climate Conditions. *Energy Convers. Manag.* **2016**, *127*, 233–244. [CrossRef]
62. Guven, A.F.; Samy, M.M. Performance Analysis of Autonomous Green Energy System Based on Multi and Hybrid Metaheuristic Optimization Approaches. *Energy Convers. Manag.* **2022**, *269*, 116058. [CrossRef]
63. Barakat, S.; Samy, M.M.; Eteiba, M.B.; Wahba, W.I. Feasibility Study of Grid Connected PV-Biomass Integrated Energy System in Egypt. *Int. J. Energy Environ. Sci.* **2016**, *17*, 519–528. [CrossRef]
64. *Davis &Shirtliff Product Manual*; Davis &Shirtliff: Nairobi, Kenya, 2022.
65. SUNTECH POWER. ULTRA S 144 Half Cell Mono Facial Module 335-455W Data Sheet. 2021. Available online: https://www.suntech-power.com (accessed on 21 April 2026).
66. WECO Dual Voltage 5k3 Data Sheet. WECO Sri Italia—Firenze. Available online: www.wecobatteries.com (accessed on 28 April 2026).
67. RENTEC JPC Lead Carbon Battery 12-200. RENTECH Renewable Technologies. Available online: www.rentech.co.za (accessed on 28 April 2026).
68. Kirloskar Oil Engines Limited. Available online: https://www.kirloskaroilengines.com/products/power-gen (accessed on 2 May 2026).
69. Mulenga, E.; Kabanshi, A.; Mupeta, H.; Ndiaye, M.; Nyirenda, E.; Mulenga, K. Techno-Economic Analysis of Off-Grid PV-Diesel Power Generation System for Rural Electrification: A Case Study of Chilubi District in Zambia. *Renew. Energy* **2023**, *203*, 601–611. [CrossRef]

70. Orr, J.; Gibbons, M.; Arnold, A. *A Brief Guide to Calculating Embodied Carbon*; Green Building Council of Australia: Sydney, Australia, 2021.
71. Reichel, C.; Müller, F.; Friedrich, P.; HorcegMiteg, J.; Neuhous, T. CO_2 Emissions of PV Module Design: Impact of Module Design and Production Location. *Renew. Energy* **2021**, *165*, 1234–1245.
72. Dodd, N.; Espinosa Martinez, M.D.L.N.; Van Tichelen, P.; Peeters, K.; Soares, A. *Preparatory Study for Solar Photovoltaic Modules, Inverters and Systems*; EUR 30468 EN; Publications Office of the European Union: Luxembourg, 2020; ISBN 978-92-76-26345-6. [CrossRef]
73. Benton, K.; Yang, X.; Wang, Z. Life Cycle Energy Assessment of a Standby Diesel Generator Set. *J. Clean. Prod.* **2017**, *165*, 1071–1080. [CrossRef]
74. Morini, A.A.; Ribeiro, M.J.; Hotza, D. Carbon Footprint and Embodied Energy of a Wind Turbine Blade—A Case Study. *Int. J. Life Cycle Assess.* **2021**, *26*, 1563–1574. [CrossRef]
75. Peiseler, L.; Schenker, V.; Schatzmann, K.; Pfister, S.; Wood, V.; Schmidt, T. Carbon Footprint Distributions of Lithium-Ion Batteries and Their Materials. *Nat. Commun.* **2024**, *15*, 10301. [CrossRef] [PubMed]
76. Lakhouit, A.; Alhathlaul, N.; El Mokhi, C.; Hachimi, H. Assessing the Environmental Impact of PV Emissions and Sustainability Challenges. *Sustainability* **2025**, *17*, 2842. [CrossRef]
77. Thomson, R.C.; Harrison, G.P. *Life Cycle Costs and Carbon Emissions of Offshore Wind Power*; University of Edinburgh: Edinburgh, UK, 2015.
78. Schmied, M.; Knörr, W. *Calculating GHG Emissions for Freight Forwarding and Logistics Services*; INFRAS: Zurich, Switzerland, 2012.
79. Samy, M.M.; Barakat, S. *A Hybrid PV-Biomass Generation Based Micro-Grid for the Irrigation System of a Major Land Reclamation Project in Kingdom of Saudi Arabia (KSA)—Case Study of Albaha Area*; IEEE: Piscataway, NJ, USA, 2018; ISBN 978-1-5386-5186-5.
80. Pillot, B.; Muselli, M.; Poggi, P.; Haurant, P.; Hachimi, I.S.E. On the impact of the global energy policy framework on the development and sustainability of renewable power systems in Sub-Saharan Africa: The case of solar PV. *Sustain. Energy Technol. Assess.* **2017**, *52*, 102148. [CrossRef]
81. International Renewable Energy Agency (IRENA). *Renewable Mini-Grids: Innovation Landscape*; IRENA: Abu Dhabi, United Arab Emirates, 2019. Available online: https://www.irena.org/-/media/Files/IRENA/Agency/Publication/2019/Sep/IRENA_Renewable_mini-grids_2019 (accessed on 28 April 2026).
82. World Bank. *Mini Grids for Half a Billion People: Market Outlook and Handbook for Decision Makers*; World Bank: Washington, DC, USA, 2019. Available online: https://www.esmap.org/publications/2019-mini-grids-half-billion-people-market-outlook-and-handbook-decision-makers (accessed on 28 April 2026).
83. International Renewable Energy Agency (IRENA). *Pay-As-You-Go Models: Innovation Landscape Brief*; IRENA: Abu Dhabi, United Arab Emirates, 2020. Available online: https://www.irena.org/-/media/Files/IRENA/Agency/Publication/2020/Jul/IRENA_Pay-as-you-go_models_2020 (accessed on 28 April 2026).
84. Akhade, N.Z.; Argiolas, A. Demand Stimulation for Sustainability of Minigrids in Global South—A Case Study from Zambia. In Proceedings of the 2025 IEEE Power Electronics Society International Decentralized Energy Access Symposium (IDEAS), Bali, Indonesia, 7–9 January 2025; pp. 1–5. [CrossRef]
85. Tamele, B.Z.S.; Wassie, Y.T.; Tsamba, A.J.; Ahlgren, E.O. Electricity consumption and its determinants in rural Mozambique—At the edge of the electricity grid. *Energy Sustain. Dev.* **2025**, *85*, 101662. [CrossRef]
86. Araoye, T.O.; Ashigwuike, E.C.; Umar, S.A.; Eronu, E.M.; Ozue, T.G.; Egoigwe, S.V.; Mbunwe, M.J.; Odo, M.C.; Ajah, N.G. Modeling and Optimization of a PV-Diesel-Biogas Hybrid Microgrid Energy System for Sustainability of Electricity in Rural Area. *Int. J. Power Electron. Drive Syst.* **2023**, *14*, 1855–1864. [CrossRef]
87. Chisale, S.W.; Eliya, S.; Taulo, J. Optimization and Design of Hybrid Power System Using HOMER Pro and Integrated CRITIC-PROMETHEE II Approaches. *Green Technol. Sustain.* **2023**, *1*, 100005. [CrossRef]
88. Mwakitalima, I.J.; Rizwan, M.; Kumar, N. Integrating Solar PV Power Source and Biogas Energy-Based System for Increasing Access to Electricity in Rural Areas of Tanzania. *Int. J. Photoenergy* **2023**, *2023*, 7950699. [CrossRef]
89. Li, J.; Liu, P.; Li, Z. Optimal Design and Techno-Economical Analysis of a Hybrid Renewable Energy System for Off-Grid Power Supply and Hydrogen Production: A Case Study of West China. *Chem. Eng. Res. Des.* **2022**, *177*, 604–614. [CrossRef]
90. Samikaanu, R.; Oladiran, M.T.; Gamariel, G.; Makepe, P.; Keisang, K.; Ladu, N.S.D. An Assessment and Design of a Distributed Hybrid Energy System for Rural Electrification: The Case for Jamataka Village, Botswana. *Int. Trans. Electr. Energy Syst.* **2022**, *2022*, 4841241. [CrossRef]
91. Perez, D.R.; Canete, A.H.; Solar, D.A.; Salgado, C.V.; Navarro, T.G. Modelling Biomass Gasifiers in Hybrid Renewable Energy Microgrids: A Complete Procedure for Enabling Gasifiers Simulation in HOMER. *Renew. Energy* **2021**, *174*, 501–512. [CrossRef]
92. Oloo, F.; Molefyane, B.; Rampokanyo, M. Modeling and Optimization Studies for Generator Dispatch Strategies for Deployment of an Off-Grid Micro-Grid in South Africa. In *Proceedings of the 2020 6th IEEE International Energy Conference (ENERGY Con)*; IEEE: Piscataway, NJ, USA, 2020. [CrossRef]

93. Virdy, S.S.; Yamba, F.D.; Mishra, M.; Simate, I.N.; Ramesh, M.; Kaoma, M.; Luwaya, E.; Tembo, S.; Gheewala, S.H. Techno-Economic Feasibility Analysis of Hybrid Renewable Energy System for Off-Grid African Communities: Insights from a Zambian Case Study. *Int. J. Renew. Energy Dev.* **2026**, *15*, 172–190. [CrossRef]
94. Schulte, J.; Figgener, J.; Woerner, P.; Sauer, D.U. Forecast-Based Charging Strategy to Prolong the Lifetime of Lithium-Ion Batteries in Standalone PV Battery Systems in Sub-Saharan Africa. *J. Energy Storage* **2023**, *50*, 104123. [CrossRef]
95. Yamegueu, D.; Nelson, H.T.; Boly, A.S. Improving the Performance of PV/Diesel Microgrids via Integration of a Battery Energy Storage System: The Case of Bilgo Village in Burkina Faso. *Energy Sustain. Soc.* **2024**, *14*, 48. [CrossRef]
96. Mandelli, S.; Brivio, C.; Colombo, E.; Merlo, M. A Sizing Methodology Based on Levelized Cost of Supplied and Lost Energy for Off-Grid Rural Electrification Systems. *Renew. Energy* **2016**, *89*, 475–488. [CrossRef]
97. Rural Electrification Authority (REA). Rural Electrification Master Plan for Zambia (2025–2030): Towards Universal Energy Access with Technical Support from National Rural Electric Cooperative Association (NRECA) International. Available online: www.rea.org.zm (accessed on 29 April 2026).
98. Nnachi, G.U.; Richards, C.G.; Hamam, Y. A Comprehensive State-of-the-Art Survey on Green Hydrogen Economy in Sub-Saharan Africa. *Preprints* **2024**. [CrossRef]
99. Msweli, N.; Nnachi, G.U.; Richards, C.G. A Review of Green Hydrogen Technologies and Their Role in Enabling Sustainable Energy Access in Remote and Off-Grid Areas Within Sub-Saharan Africa. *Energies* **2025**, *18*, 5035. [CrossRef]
100. Nnachi, G.U.; Richards, C.G.; Hamam, Y. Appraising the benefits of investing in green hydrogen in Sub-Saharan Africa's energy mix. In Proceedings of the 2025 33rd Southern African Universities Power Engineering Conference (SAUPEC), Pretoria, South Africa, 29–30 January 2025; pp. 1–6. [CrossRef]

Disclaimer/Publisher's Note: The statements, opinions and data contained in all publications are solely those of the individual author(s) and contributor(s) and not of MDPI and/or the editor(s). MDPI and/or the editor(s) disclaim responsibility for any injury to people or property resulting from any ideas, methods, instructions or products referred to in the content.